Towards time resolved single spin measurements.

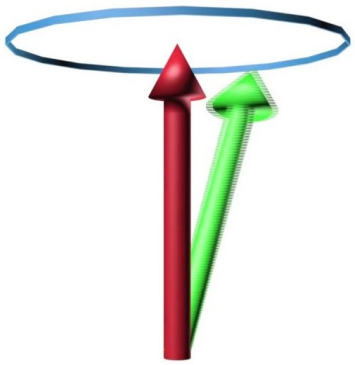

THESIS

submitted in partial fulfillment of the
requirements for the degree of

MASTER OF SCIENCE
in
PHYSICS

Author :	Tjerk Benschop
Student ID :	1406035
Supervisor :	Dr. M.P. Allan
2^{nd} corrector :	”

Leiden, The Netherlands, October 11, 2017

Towards time resolved single spin measurements.

Tjerk Benschop

Huygens-Kamerlingh Onnes Laboratory, Leiden University
P.O. Box 9500, 2300 RA Leiden, The Netherlands

October 11, 2017

Abstract

In this work, the possibility to measure time- and spatially resolved spin fluctuations using Scanning Tunneling Microscopy is investigated. By using an impedance matching circuit as described in [1], the bandwidth of conventional STM can be increased opening up possibilities for new kinds of experiments. When combined with the technique of spin-polarized STM, it theoretically becomes possible to track spin states of individual atoms. Here, we present an overview of existing literature on this topic and propose several experiments to test this hypothesis. Finally, with a python simulation, we test the viability of EPR-STM measurements on a single atom and provide directions to expand upon this work.

Contents

Version of October 11, 2017– Created October 11, 2017 - 16:15

Chapter 1

Introduction

High temperature superconducting copper-oxide compounds, or cuprates, have been know to man since 1986. Currently, almost thirty years later, it is still not fully understood how superconductivity survives up till such high temperatures, but there are plenty of rumors about strong spin interactions that mediate the pairing mechanism in these type of compounds, enhancing their Tc. Up till now, there is no experimental data of local spin fluctuations with high spatial and temporal resolution. This is something that we would very much like to change in the future.
To tackle this problem, because we demand high spatial resolution, the first type of measurement device that comes to mind, is a Scanning Tunneling Microscope (STM). Being known to achieve atomic resolution with ease, it should be the perfect device for these type of measurements. When combined with a spin polarized tip (SP-STM), the conventional STM is capable of measuring the magnetic structure of samples with atomic precision. There is however also a big downside to STM measurements: Due to the nature of the apparatus, its temporal resolution is fairly poor ($\sim kHz$). Since relevant timescales for spin fluctuations in high-Tc compounds have been predicted to be in the range of $\sim GHz$ or even $\sim THz$, the temporal resolution of STM should first be improved in order to open up the possibility of measuring them. One solution for this is to mount a cryogenic, low-noise amplifier close to the tip of the STM amplifying the signal before it is low pass filtered [1]. If the amplification is big enough, we retain the possibility to measure small signals with a bandwidth that depends on the amplifier itself. In this report, we would like to investigate the possibility to measure properties of single spin systems in real time.
In chapter 2, we begin by reviewing some existing literature on measurements of temporal evolution of single spin systems. Following these re-

Version of October 11, 2017– Created October 11, 2017 - 16:15

views, we outline some ideas for experiments in chapter 3 that could possibly be performed using a commercial low-temperature STM provided with a magnet and RF electric matching circuitry. In chapter 4, we continue by providing some theory to support these experiments. Chapter 5 focuses on a simulation of the tunneling current that we expect to measure in the system described in chapter 3. Finally, in chapter 6, we provide some points for future research.

Chapter 2

Literature on temporal single spin measurements

The development of a STM capable of measuring spin fluctuations with atomic resolution will be a long term objective. As was already expressed in the introduction of this report: It is the time resolution of scanning tunneling microscopes that severely limits its capabilities and prevents us from reaching this goal. To overcome this obstacle, we propose to build a high frequency amplifier close to the tip in order to still measure radio signals as described elsewhere [1]. In this report, we will focus on creating a proof of principle experiment, hopefully demonstrating some of the possibilities of a STM equipped with a RF amplifier. Furthermore, we hope to be able to measure the temporal evolution of a single (possibly driven) spin. This means that the aim of this experiment will be to measure relaxation times of a single spin in "real time" and possibly measure Rabi oscillations of a single spin.
We begin this report by reviewing some important literature, on which the experiment will be based.

2.1 Measurement of Fast Electron Spin Relaxation Times with Atomic Resolution

In 2010, Loth et al. [2] first introduced an all electric pump probe technique, allowing them to measure the longitudinal relaxation time (T1) of Fe-Cu dimers on a Cu_2N layer suspended on a Cu(100) bulk sample. The CuN layer serves as a decoupling layer between the Fe spin and the conduction electrons of the bulk Cu substrate. Furthermore the Cu atom ad-

jacent to the Fe atom enlarges the local magnetic anisotropy felt by the Fe atom. Both these elements together make for the fact that the Fe atom has relatively long relaxation (T1) time, on the order of 200ns.
The idea of the pump- probe measurement technique applied in this paper is the following: First, a pump pulse with a fixed bias voltage excites the spin state of in this case the Fe atom. A time Δt later, a second probe pulse with a much lower bias voltage measures the relative spin polarization of the Fe spin with respect to its ground state (figure 2.1). By repeating this process for various Δt, the time dependent spin relaxation of a single atom can be measured. The magnitude of the pump- and probe pulse are different for each system. Luckily, using IETS (section 3.2), the energy spectrum of the individual atom can be measured and correct values for the pump and probe pulse can be determined experimentally within the same setup. The pump pulse should satisfy $eV_{pump} \geq \Delta E$, where ΔE is the energy difference between the ground state and excited state of the spin system. Complementary, the probe pulse should fulfill $eV_{probe} < \Delta E$ to avoid re-exciting the spin.

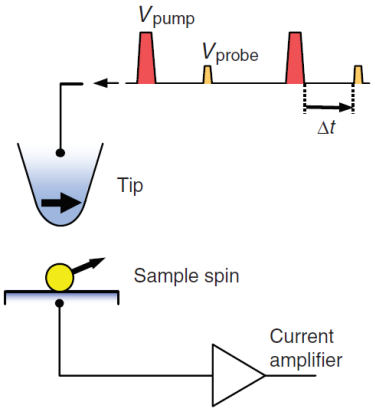

Figure 2.1: *Scheme of the pump- probe measurement technique used in ref 2. A pump pulse excites the spin state of the adatom in the tunnel junction. After waiting Δt, a secondary probe pulse measures the orientation of the adatom spin. By varying Δt, the evolution of the spin relaxation process can be tracked in time. Figure taken from reference [2].*

Setupwise, Loth et al. use a STM with a spin-polarized tip at a temperature of 0.6K. Furthermore, a magnetic field of 7T is applied perpendicular to the sample. For Fe-Cu dimers, this means that the field is applied parallel to the magnetic anisotropy axis, enhancing the level splitting of the energy eigenstates of the Fe atom. The tip is polarized parallel to the

applied magnetic field. Thus in this case, the tip is polarized perpendicular to the sample and parallel to the magnetic anisotropy axis. Since the ground state of the Fe atom has a spin polarization parallel to the magnetic anisotropy axis, upon excitation, the spin of the Fe atom becomes misaligned with the tip polarization. Hence, in the relaxation window of the Fe atom, a decrease in tunnel current is observed (figure 2.2).

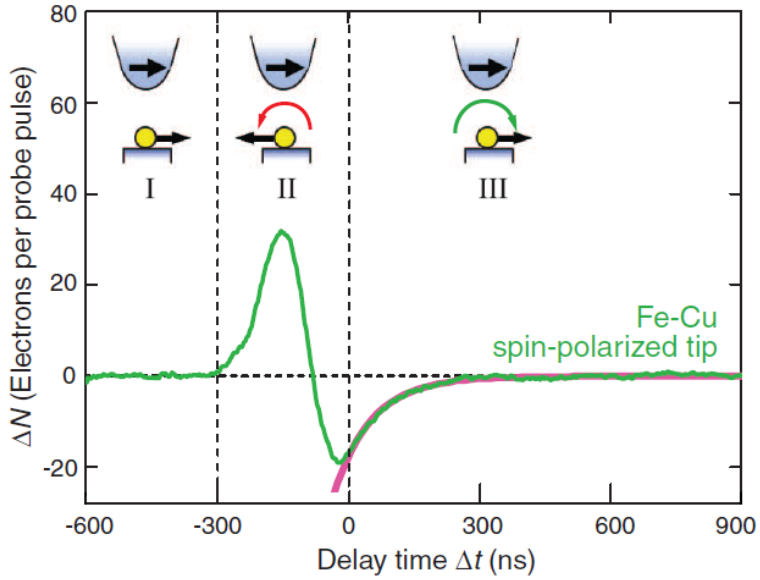

Figure 2.2: *Measured decrease in tunneling electrons as function of Δt, i.e. time between pump- and probe pulse. By fitting an exponential to the slope at $t = 0$, T1 can be obtained (red line). Data and image taken from reference [2].*

2.2 Electron Paramagnetic Resonance of individual atoms on a surface

In 2015, Baumann et al. [3] managed to do an Electron Paramagnetic Resonance experiment on a single iron atom placed on top of a single monolayer of MgO. The monolayer was grown on Ag(100) by bombarding the surface with manganese ions in an oxygen environment. Similar to the CuN layer in the previous paper, the MgO layer decouples the Fe spin from the silver substrate conduction electrons and introduces an

anisotropic magnetic environment, increasing the lifetime of spin states of the Fe-atom. However, the direction of the magnetic easy axis of the Fe spin is different from the previous case. When placing an Fe spin on top of MgO, the anisotropy axis points perpendicular to the surface and parallel to the tunnel junction.

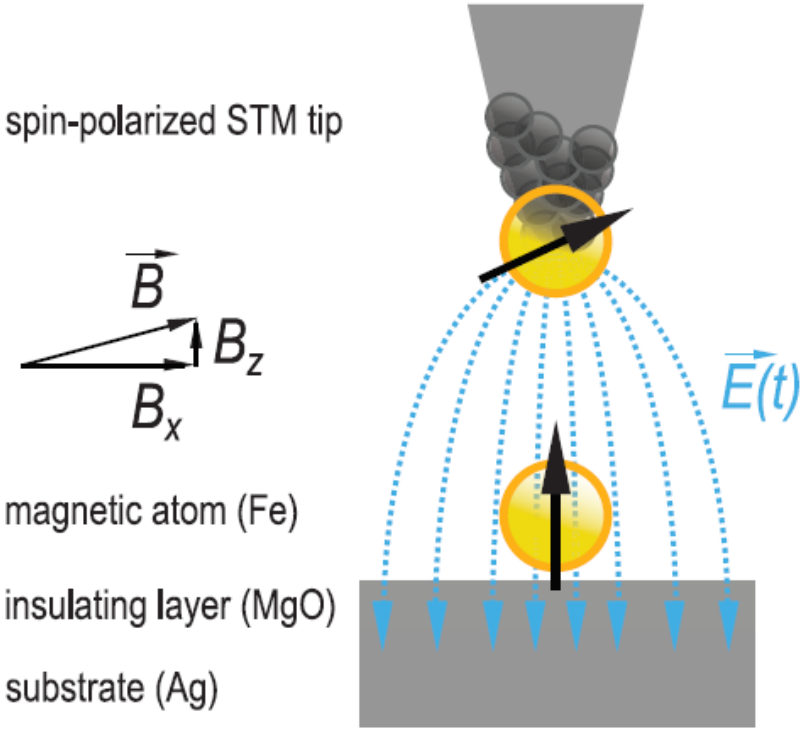

Figure 2.3: *Schematic overview of the setup used by Baumann et al. [3] to perform the EPR measurement on a single Fe atom using STM. The tip is polarized parallel to the magnetic field, whereas the adatom spin states mostly follow the anisotropic magnetic environment provided by the sample. An alternating electric field was applied between tip and sample to drive the transition between two spin states of the Fe adatom. Figure taken from reference [3]*

In this experiment, an external magnetic field was applied mostly parallel to the sample thus pointing perpendicular the anisotropy axis. This was achieved by having a magnet creating a parallel field and slightly tilting the sample ($\pm 2^\circ$). The perpendicular component (parallel to the anisotropy axis) ensures a finite level splitting, whereas the parallel component mixes the states. Having the majority of the field pointing parallel, the tip is also polarized parallel to the sample surface.

Furthermore, an oscillating electric field was applied between the tip and sample in order to drive a transition between the ground state of the atom and its first excited state ($\Delta E \approx 100\mu eV \approx 25$ GHz). When measuring the DC tunneling current and sweeping the frequency of the AC electric field, upon resonance, an increase in DC tunneling current is observed ($\pm$ 100 fA). Intuitively, this can be explained by the Rabi model (chapter 2). Upon applying the electric field, the state of the atom oscillates between a ground state and an excited state. In this case, the ground state has a spin component pointing mostly parallel to the anisotropy axis, whereas the excited state' spin component is more aligned with the tip polarization. In turn, when the Rabi oscillations have maximum amplitude, i.e. zero detuning, the excited state of the atom is on average populated more than in the case of finite detuning. Hence, for zero detuning, an increase in DC tunnel current is observed.

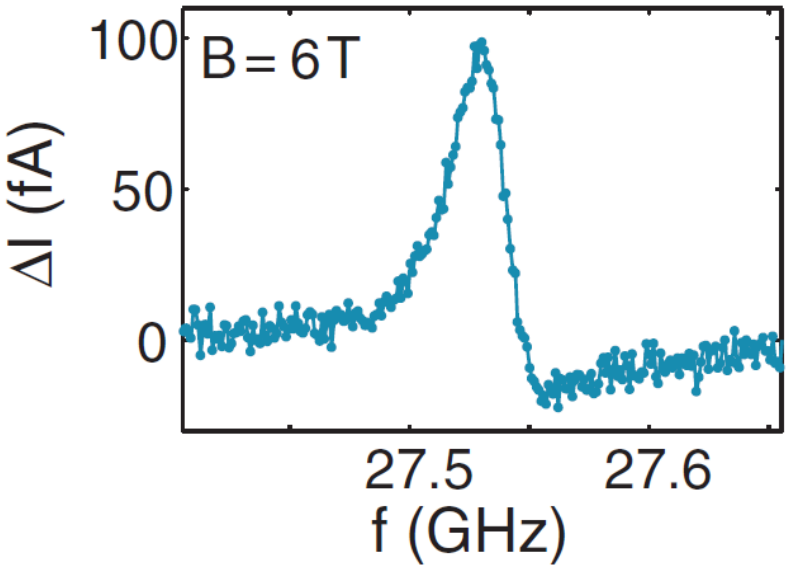

Figure 2.4: *Relative increase in DC tunneling current as a function of frequency of the applied electric field as measured by Baumann et al. [3]*

Mathematically, this was explained by Berggren et al. [4]. In this paper, it is shown that the total tunnel current can be divided into three separate components. The second component is an alternating current. When calculating the average of the total current, it can be shown that for zero detuning, it is this second component that becomes DC and explains the increase in DC tunnel current.

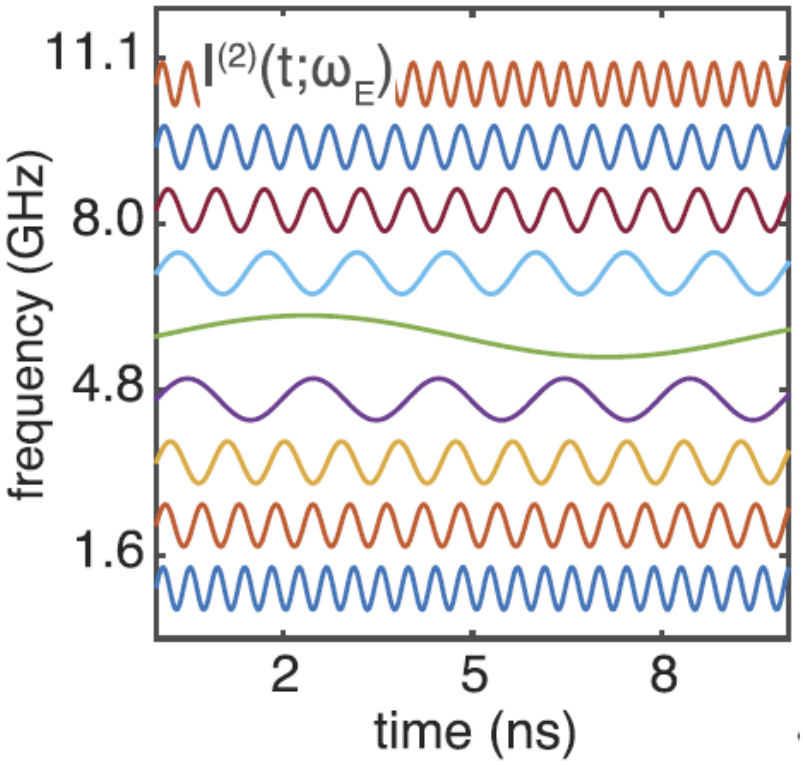

Figure 2.5: *Averaged 2^{nd} component of the total tunneling current as a function of time for different applied field frequencies (ω_e). When the field is applied resonantly, the average of this component of the current becomes DC. Figure taken from reference [4]*

From the peak in the DC tunnel current versus frequency of the applied electric field (fig 2.4), T2 and the Rabi frequency were derived. Furthermore, T1 was measured with the pump- probe technique discussed in the previous paper ($T1 \approx 88\mu s, T2 = 210ns, \Omega = 2.6rad/\mu s$).
It is important to observe that this same experiment was also attempted with Co atoms, instead of Fe atoms. Driving the transition for Co atoms proved impossible, which was later explained by Berggren et al. [4]. For half integer spin particles (such as Cobalt atoms), the transition between the ground- and excited state requires a transfer of spin angular momentum. This cannot be provided by the applied, linearly polarized electric field, and thus, it is impossible to do EPR measurements on particles with half integer spins. Since Fe has S=2, it does not suffer this problem.

2.3 Control of the millisecond spin lifetime of an electrically probed atom

One year after the paper of Baumann et al [3], in 2016, Paul et al. [5] published a paper about the same system, except with variable thickness of the MgO film. They observed that for a system with $>$ 2 Ml of MgO, the T1 time could be increased all the way to the *ms* range.
Their setup consists of a Ag(100) substrate, similar to the setup in Baumann et al. A MgO film is grown on top of the substrate, and individual Fe atoms are placed on different patches of the MgO film with variable thickness. The position of the Fe atoms on the MgO surface is manipulated with the STM tip. The magnetic field is applied perpendicular to the surface, i.e. parallel to the magnetic anisotropy axis.
To measure the T1 time of different atoms, the same pump- probe technique demonstrated by Loth et al. [2] was used. It is also noteworthy that for an Fe atom on top of 2Ml MgO, a periodic modulation of the tunnel current was observed in the otherwise DC signal. This modulation corresponds to the excitation and relaxation of a spin state of the Fe atom (fig 2.6).

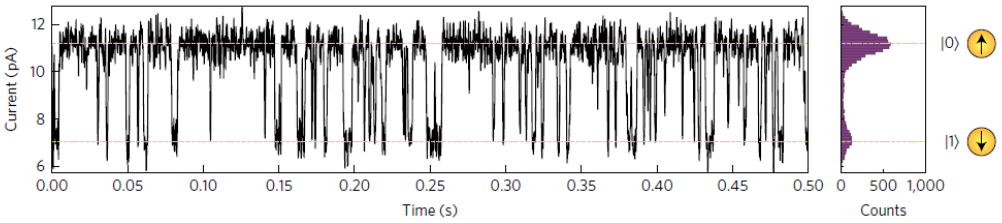

Figure 2.6: *Spin polarized tunneling current as measured with a SP tip above a single Fe adatom. The oscillation in the current can be explained by the excitation of a spin state of the adatom due to inelastically tunneling electrons. As a result of this, the adatom polarization is less aligned with the tip polarization, resulting in an increase in magneto-resistance of the tunnel junction. Upon relaxation of the excited state, the current is restored to its original value. Assuming the adatom is instantly excited after relaxation, the oscillations in the current should provide a measure for the T1 time of the excited state. Figure taken from reference [5].*

2.4 Large Magnetic Anisotropy of a Single Atomic Spin Embedded in a Surface Molecular Network

A few years before the publication of the work by Loth et al., in 2007, Hirjibehedin et al. [6] published a paper on the magnetic anisotropy effect of a CuN layer on a surface adatom which was either Fe or Mn. By using IETS (section 4.2), they measured the energy spectrum of the adatom and compared it to their theoretical expectations. They found, that even though the molecular binding environment of an Fe atom does not differ very much from that of a Mn atom, the magnetic anisotropy field of the two individual systems was very different. Where the magnetic easy axis of an Fe atom on CuN points almost parallel to the surface, the easy axis of a Mn atom on the same surface was found to point perpendicular to it. This is an important conclusion in the sense that if we are to come up with an experiment to measure the properties of a single adatom spin of an arbitrary element, we should also be able to measure the energy spectrum of the adatom within the same setup seeing as we cannot necessarily compare our system with existing literature due to the criticality of these systems. Luckily, following this paper, measuring the energies of the spin states is just a matter of doing a differential conductance measurement ($\frac{dI}{dV}$). We should keep in mind however that the energy resolution of IETS is given by $5.4k_bT$, corresponding to the thermal broadening of the tip state (double convolution of an infinitely sharp level with the Fermi distribution). This means that the level pairs used in the EPR experiment ($\sim$ 100 μeV) will be practically impossible to detect. This does not matter that much, but we should be able to detect higher lying energy states ($\sim$meV) in order to determine the degree of polarization of the tip (section 3.4).

2.5 Direct Observation of the Precession of Individual Paramagnetic Spins on Oxidized Silicon Surfaces

In 1989, Manassen et al. [7] claimed to have observed the precession of a single spin around an applied magnetic field (Larmor precession). The reason we are briefly highlighting this paper here is because it has a slightly different approach from the papers referred to in the sections above. The difference is that detection happens without a spin polarized tip. Even so,

a Larmor precessing spin induces a small modulation of the tunneling current at the Larmor frequency $\omega_l = -\gamma B$, where γ is the gyromagnetic ratio and B is the magnitude of the applied magnetic field. This modulation is detected here using a RF matching circuit and a spectrum analyzer.

2.6 Overview

In this section, we will give a schematic overview of the key points of the papers presented in this chapter.

Title	Key features
Measurement of Fast Electron Spin Relaxation Times with Atomic Resolution	• Pump- probe measurement technique to measure T1 of single Fe-Cu dimers.

Electron Paramagnetic Resonance of individual atoms on a surface	• By superimposing an AC bias to the conventional DC bias, the atom under study can be driven between two of its spin states. In this paper, Fe/Co atoms are studied on a single layer of MgO, on top of a bulk Ag(100) substrate. • When the transition is resonantly driven, an extra component in the DC tunneling current appears. • By sweeping the frequency of the applied field, the energy level splitting between the two states can be determined. • In addition to this, from the shape of the DC current as a function of applied field frequency, Baumann et al.[3] claims to be able to derive the T2 time and the Rabi frequency.
Control of the millisecond spin lifetime of an electrically probed atom	• By varying the thickness on the insulating film on the sample, the T1 time of the atom under study can be tuned. • The stray field of the SP tip influences the T1 time of spin excited states: tip- sample distance is an important parameter.

Large Magnetic Anisotropy of a Single Atomic Spin Embedded in a Surface Molecular Network	• The chemical binding environment of the surface adatom with the insulating film determines in first principle the direction of the easy magnetization axis of the adatom. • Even though certain adatoms can have a very similar chemical environment, their magnetic environments can differ substantially. (in this paper; Fe on CuN has an easy axis parallel to the sample surface, whereas Mn on CuN has an easy axis perpendicular to the surface) • Using the IETS technique (section 4.2), the energy levels of the spin excited states of the atom under study can be measured.
Direct Observation of the Precession of Individual Paramagnetic Spins on Oxidized Silicon Surfaces	• Even without a SP tip, a small AC modulation of the tunneling current can be measured that results from the Larmor precession of single spins.

Chapter 3

Proof of principle experiment

Based on the literature covered above, we will now propose an experiment in which we try measure the relaxation times of a single spin and/or Rabi oscillations.

3.1 Parameter space within our STM setup

In this section, we describe the possibilities in our own STM setup regarding single spin measurements similar to the experiments described above. In order to realize such experiments, special attention needs to be paid to:

- Possible contamination of the vacuum: we would like to maintain the UHV environment in our system. This means that our possibilities regarding sample growth are limited.
- The possibility to to EPR measurements on the sample: even if we just plan on measuring the T1 time of a single atom, it would still be nice to keep open the possibility to do EPR measurements in the future with preferably the same sample.
- In our STM setup, we are limited to magnetic fields up to 9T, applied perpendicular to the sample.
- There are different techniques for creating a SP tip, for example the procedure in reference [8], where a SP tip is made by either scanning the surface or slightly indenting the tip on the surface of an $Fe_{1+y}Te$ compound. To do experiments on the single atom systems would then require us to create the SP tip followed by a sample exchange.

This would require a highly stable tip, on which we would not like to gamble.

As a result of this, we propose the following experimental environment:

- It is rather inconvenient to grown MgO films in our STM because it requires filling the system with oxygen. This means that the vacuum chamber will be polluted which we would like to avoid. Therefore we would like to use Cu(100) with a CuN film, since the film is relatively easy to grow with a relatively small amount of pollution (section 3.2).

- In order to be able to do EPR measurements where we drive an atomic transition with an alternating electric field between tip and sample, we choose to evaporate individual iron atoms (S=2) on the sample.

- The magnetic field in our STM setup is limited to 9T perpendicular to the sample. In order to create some in plane magnetic field, we could tilt the sample under a slight angle. We estimate a maximum tilt angle of 5°, in order to still be able to do STM.

- It seems easiest to first prepare the single spin system and thereafter pick up a single magnetic adatom to polarize the tip (section 3.3).

3.2 Sample preparation

Creating a CuN layer on top of Cu(100) can be done in multiple ways. In this section, we describe the method used in a paper by Leibsle et al.[9]. This paper studied the Cu(100)-c(2x2)N surface structure, which is the surface we would like to prepare.

Recipe:

1. Clean the Cu(100) sample by repeated cycles of argon ion bombardment and annealing (600K). The authors of Leibsle et al. use LEED to verify the cleanliness of the surface. Our system is not provided with a LEED setup, however, we can check the quality of the surface by taking large scale topographs if deemed necessary.

2. Ion bombard the crystal with nitrogen ions. This can be done at room temperature, at a pressure of 3.6×10^{-4} mbar. The nitrogen gas used by Leibsle et al. was of 99.999% purity and their ion gun had a beam energy of 500 eV.

3. Heat the sample to 600K.

4. Use the evaporator to evaporate single Fe atoms onto the sample. The exact settings for the evaporator need to be tested to achieve the best results. Furthermore, for example in the paper by Baumann et al. [3], they cool the sample to 4K when evaporating the Fe atoms. It is not known if this is necessary, but it might be worth looking into a way to cool the sample holder during evaporation.

3.3 Creating a spin polarized tip

To create a spin polarized tip on these single spin samples, one has to start this process by coating the tip with a metal. This can be best achieved prior to the sample preparation using the clean Cu(100). By indenting the tip (PtIr) on the surface, Cu atoms will coat the apex of the tip. Then, the sample can be retracted from the STM head in order to commence the sample preparation (section 3.2). The metallic coating of the tip is necessary in order to reduce the lifetime of the excited spin states of the polarized atom on the tip. Where the insulating layer on the sample (here CuN) extends the life- and coherence times of the adatom placed on top, we want the tip polarization to remain constant during our measurements. The metallic coating of the tip achieves this by ensuring a strong coupling between the tip spin and the conduction electrons in the tip. Excited states of the tip spin have an expected lifetime $<$ ps, hence the tip spin can be considered to have a constant polarization in most experiments.
To transfer an Fe atom to the tip, we follow the procedure applied by Baumann et al[3]. The tip should be positioned above an adatom and brought close to the sample ($\sim$ 1 MΩ junctionresistance). Then, the tip should be

retracted whilst applying a large voltage bias ($\sim$ 0.55 V). Typically, this procedure should be repeated ± 5 times in order to successfully transfer the adatom to the tip. It should also be noted that this technique can best be attempted with a blunt tip. In order to blunt the tip, we can slightly indent it on the CuN surface, making sure not to damage the surface too much. To test if the adatom has been transferred successfully, the degree of tip polarization should be measured as described in the next section.

3.4 Experimental procedure

Once the single spin systems are created on the sample and a spin polarized tip has successfully been made, the sample should first be characterized in order to start time resolved measurements. This is necessary in order to know the direction of the magnetic anisotropy axis. According to Hirjibehedin et al. [6], the magnetic anisotropy axis of an Fe atom on CuN lies mostly parallel to what they define as the N- direction. In order to clarify this, we take a look at the topograph made by Hirjibehedin et al. of Fe on CuN (fig 3.1).

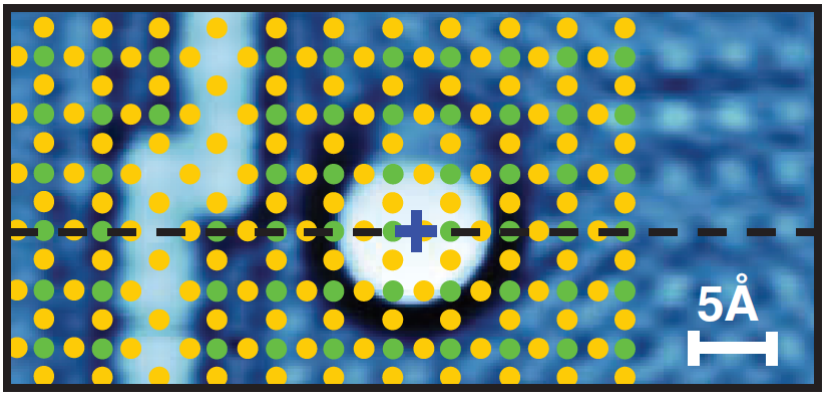

Figure 3.1: *Topograph of the single spin system of Fe adatoms on CuN created by Hirjibehedin et al. [6]. Marked by the blue cross is the position of the Fe adatom on the surface. For clarity, the Cu atoms (yellow) and the N atoms (green) were drawn in the picture. The Fe atom binds on a copper site, next to two N atoms. We define the N- direction, similar to Hirjibehedin et al.[6], parallel to the line intersecting the 2 neighboring N atoms of the Fe adatom.*

From figure 3.1, it becomes clear that the Fe adatoms like to bind on a Cu site next to two nitrogen atoms. We define the direction parallel to the line intersecting these two nitrogen atoms as the N- direction, following the

convention of Hirjibehedin et al.[6]
A finite amount of magnetic field can be applied in this N-direction to tune the level splitting of adatom states. Since we can only apply field perpendicular to the sample, the only way to achieve this is by tilting the sample prior to mounting it in the STM. Since there is no way to know a priori what direction will become the N-direction, the sample should be tilted on a corner before inserting the sample to ensure a finite tilt angle over both directions.
Another option would be to, if possible, install the magnet under an angle. This would be preferred since we are not sure how tilting the sample will affect scanning and we need to have atomic resolution in order to determine the N- direction.
Once the N-direction has been established, the magnetic field can be applied. The component parallel to the N- direction tunes the level splitting between the spin states of the adatom, whereas the component orthogonal to the N- direction mixes the states. Furthermore, since the latter component will be larger than the former, it will be mostly this component that can be used to enhance the degree of polarization of the tip. The exact values for the applied magnetic field need to become apparent from simulations (chapter 4).
After a magnetic field is applied, the setup procedure is completed and we can begin characterizing the sample. We start by doing an Inelasting Electron Spectroscopy Measurement (section 4.2), in order to characterize the energy levels and spin states of the adatom. Furthermore, from the $\frac{dI}{dV}$ obtained, the degree of spin polarization of the tip can be measured. Following Loth et al. [10], the degree of polarization can be derived from the $\frac{dI}{dV}$ curve. Because the tip is polarized, the density of states can be split up into two spin components, i.e. up and down electrons. To excite a spin state in the adatom which requires spin angular momentum transfer, for example $S = +2 \rightarrow S = +1$, an electron from either the tip or the sample will have to transfer a quantum of spin to the adatom, depending of the polarity of the applied bias.

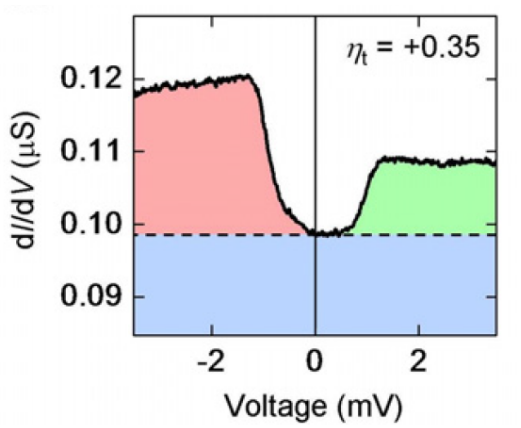

Figure 3.2: *Example data of an IETS measurement using a spin polarized tip. This data was taken from Loth et al [10]. They measured dI/dV with a spin polarized tip on a Mn atom on top of a CuN surface. It is really clear that the conductance for negative bias at the inelastic transition (red), is roughly 10% larger than at positive bias (green). It is this difference that allows us to infer the polarization of the tip.*

Since in our case the tip is spin polarized (meaning there is a difference in D.O.S. for up- and down electrons) and the substrate is not polarized, the height of conductance step corresponding to the inelastic transition between the final adatom state ($|\Phi_f\rangle$) and the initial adatom state ($|\Phi_i\rangle$) will be different for positive and negative bias. From the height difference in the conductance steps at positive and negative bias (fig 3.2), the degree of spin polarization can be inferred according to:

$$P_t = \frac{1}{\eta_s}\frac{G^+ - G^-}{G^+ + G^-} \tag{3.1}$$

Where G^+ and G^- are the $\frac{dI}{dV}$ values of the conductance step corresponding to the inelastic transition, at positive and negative bias respectively and η_s is the polarization of the adatom spin:

$$\eta_s = \frac{|\langle\Phi_f|S^+|\Phi_i\rangle|^2 - |\langle\Phi_f|S^-|\Phi_i\rangle|^2}{2|\langle\Phi_f|S|\Phi_i\rangle|^2}$$

After this final characterization procedure has been completed, we can measure a number of physical quantities regarding the temporal evolution of a spin state. Below, we present a few ideas based on the work discussed in chapter 2 for measuring different physical quantities related to the temporal evolution of a single atom spin state.

3.4.1 Measuring T1 on a single atom

As described in section 2.1, in 2010, Loth et al. [2] first introduced a pump-probe measurement scheme in order to measure the decay time of an excited spin state. In this section, we would like to propose an alternative method for measuring this T1 time.
Instead of doing the pump- and probe measurement for several cycles, we think it is possible to measure the decay of the spin state in real time just by applying a DC bias. A requirement for this type of measurement is an extension, or shift in bandwidth, which can be achieved by using our RF-STM setup (section 4.1). If we could measure alternating current signals in the frequency range characteristic for the decay of the spin state ($\frac{1}{T_1}$), we could keep exciting the spin state by applying a DC bias voltage larger than the energy difference between the two states. In this way, electrons can inelastically excite the spin each time it relaxes back to its ground state. Assuming we apply a large enough current by approaching the sample really close, the spin is instantly re-excited after relaxation. As a result, the tunneling current will be modulated at a frequency characteristic for its relaxation time.
For Fe atoms on CuN, the T_1 time is unknown. However, for Fe-Cu dimer on CuN, the T_1 time was measured by Loth et al. in their pump-probe measurement paper [2]. They obtained a T_1 time, varying between 50 ns and 250 ns. This corresponds to $\frac{1}{50\times10^{-9}} = 20$ GHz and $\frac{1}{250\times10^{-9}} = 4$ MHz, meaning that especially in the latter case we could measure the T_1 time using our already existing RF- circuitry (after some minor modifications).
For Fe-Cu dimers, the magnetic easy axis points parallel to the sample surface. Since we are not doing EPR in this experiment, we do not have to worry about applying field perpendicular to this axis to mix the states. Hence, this experiment can be done in our STM by just applying the field perpendicular to the surface. The tip polarization aligns with the magnetic anisotropy axis, thus a decrease in tunnel current is expected to be measured upon excitation of the spin. With the RF- circuitry, we should be able to measure this current change in the MHz range. If we do not immediately detect the AC signal, it is possible that the lifetime of the selected Fe-Cu dimer is too short and falls out of our bandwidth. Hence we should try different Fe-Cu dimers at different positions on the sample since the local environment can influence the lifetime. Also junction resistances should be varied at each dimer since it was observed in Paul et al. [5] that the stray field of the tip spin can influence the lifetime of the spins quite dramatically. Therefore, it should also be mentioned that the bandwidth of the RF- circuitry should be chosen preferably in the up-

per MHz region or even redesigning the amplifier to get bandwidth in the GHz range could provide useful. Should we not detect any signal because the lifetime is too long, we could lower the junction resistance, therefore decreasing the lifetime of the excited state and increasing the frequency of the AC signal, potentially shifting it into our bandwidth.
If we attempt this experiment on individual Fe atoms, the field could still be applied perpendicular to the surface. The only difference is that now, the tip polarization is orthogonal to the magnetic easy axis resulting in an increase in tunneling current upon exciting the spin state. This is only relevant for the pump- probe measurement, but it is recommended to do this on single iron atoms before attempting the real time detection in order to tune the bandwidth of the RF- circuitry to the correct frequency range. Also, the applied field could be varied in this case to enhance state mixing an thereby potentially change the relaxation time directly. The lower the field, the less state mixing therefore the longer the lifetime, but it should be mentioned that the tip polarization of course also depends on this applied field and it is not certain what the lower limit of the applied field is in order to keep a stable tip polarization.

3.4.2 EPR on Fe adatoms

The second type of measurement we can do with Fe atoms on CuN involves applying an alternating electric field in the tunnel junction. This can be achieved by superimposing an AC bias on the standard DC bias, using for example a function generator. The AC electric field will be able to drive transitions between two states of the adatom, depending on the frequency of this applied electric field (section 4.3). Depending on how we set the DC bias, we predict the ability to measure two different phenomena:

- A change in DC tunnel current when the transition is resonantly driven. This phenomenon is in principle independent of the applied bias voltage and was experimentally measured by Baumann et al. [3]. A theoretical explanation for this was given by Berggren et al. [4] (section 4.5). From the shape of the resonance peak, T_2 and the Rabi frequency can be derived.

- An alternating current component corresponding to the Rabi oscillations of the magnetic adatom. This is something that has not been measured before and can probably only be measured when the DC bias can be kept constant in the μV range. (section 4.5)

In an EPR measurement, the magnetic field component perpendicular to the anisotropy axis enhances the spin state mixing of the eigenstates. The parallel field component is used to control the level splitting and thereby the resonance frequency of the transition.
The amplitude of the applied alternating electric field eventually determines the Rabi frequency, i.e. the rate at which the transition takes place (section 4.3). Please observe that it is necessary to vary the output power of the function generator for different frequencies taking into account the transfer function of the STM in order to get an equal electric field amplitude for all frequencies in the tunnel junction. [3], [11].

3.4.3 Overview

In this section, we give a short, schematic overview of the experiments described above. We state the main technical challenges and possible results in terms of new physics that can be learned from the experiments.

Experiment	Technical challenges	Outcome/What can we learn?
Realtime measurement of the T1 time of a single atom.	• Tunnel junction stability • Tuning of the RF circuitry	Probably we cannot learn any new physics from this type of experiment. However, if successful, this experiment will demonstrate the viability of a STM with good time resolution. Furthermore, it will provide a new method for measuring T1 times of single atoms and as a group, it will provide a way for us to get experience with these kind of samples. If we get RF ciruitry with better bandwidth and higher resonance frequency, we might also be able to do this kind of measurement on more interesting samples, provided we come up with a new way to make a SP tip.
DC EPR measurements.	• Tunnel junction stability • Controlling amplitude of the applied electric field	Since this experiment has already been conducted by Baumann et al. [3], we will not be able to learn anything new per se. Furthermore, since the technique only works for a transition between two well defined levels, it will probably not be possible in most bulk systems.

AC EPR measurements.	• Tunnel junction stability • Tuning of the RF circuitry • Requirement of μV control of the applied DC bias • Controlling amplitude of the applied electric field	Time resolved Rabi oscillations have, to our knowledge, never been measured electronically. Therefore, if this experiment succeeds, it will be the first time someone has ever done that. In terms of new physics however, the Rabi model is a really well understood concept in quantum optics. Hence, we probably will not learn any new physics from this experiment. Furthermore, since the Rabi model assumes that a spin oscillates between two well defined states, the applicability of this model becomes questionable in bulk systems.

Chapter 4

Theory

4.1 (RF-) Scanning Tunneling Microscopy

The technique of Scanning Tunneling Microscopy is based on measuring a finite tunneling current between an atomically sharp tip and a sample. This finite tunneling current is a purely quantum mechanical effect that, according to Bardeen [12], depends on the overlap between the electronic wavefunctions of the tip and sample. It is for this reason that the spatial resolution of STM is so outstandingly good, because the current will decay exponentially as a function of tip- sample distance. This means that small deviations ($\sim \mathring{A}$) can be detected as relatively large deviations in the tunnel current.
Moreover, the usefulness of STM does not end here. By freezing the feedback and measuring $\frac{dI}{dV}$, insight in the local density of states of the sample can be obtained (STS). By measuring the noise of the tunneling current (shotnoise), we can learn the properties of the charge carriers in the sample and by using a spin-polarized tip, the local magnetic structure of the sample can be analyzed. It is this last effect that we would like to apply in order to measure the spin state of individual atoms.
In the introduction, we briefly commented on one of the weaknesses of STM: its temporal resolution. The reason for this is that, especially in low-temperature UHV-STMs, the STM head is connected to room temperature current amplifiers by means of a relatively long coax cable. The problem lies with the parasitic capacitance that is introduced by this cable. This basically low-pass filters all signals coming from the STM head before it reaches the amplification stage. As a result, it becomes impossible to detect small signals $>$ 10 kHz, severely limiting the temporal resolution of

the device.
One way to overcome this problem is by introducing a small, low-noise cryogenic amplifier close to the STM head, amplifying all signals within a certain bandwidth [1]. This means that the attenuation due to the coax cable is basically negated by means of amplification before the signal reaches this low-pass filter stage. In principle, this method can open up the possibility to measure time-resolved spin fluctuations and or spin relaxation, if combined with a spin-polarized tip.

4.2 Inelastic Electron Tunneling Spectroscopy (IETS)

Inelastic Electron Tunneling Spectroscopy is a technique originally used to measure vibrational modes in molecules. Around 1990, the technique was sort of re-discovered and was first applied in a STM. Now, by combining IETS with spin polarized tips, it is possible to measure the magnetic states of samples with atomic precision.
The principle of IETS was described in section 3.4. Here, we would like to elaborate a bit more on the working principle behind IETS. For further reading, we would like to refer to reference [10].
To start off, we would like to point out that the total tunneling current inside a tunnel junction can be regarded as two individual components. One part is fully elastic, meaning that electrons tunnel from one reservoir to another without losing or gaining energy. This means that for the single spin systems described in chapter 2, the electrons do not influence the state of the adatom and either tunnel directly between the two reservoirs, or cotunnel from one reservoir through the adatom to the other reservoir, without exchanging energy or spin angular momentum. The other component, the inelastic part, contains more information since it depends on the available quantum states of the magnetic adatom. Inelastically tunneling electrons come from one reservoir, tunnel to the magnetic adatom and exchange either energy or angular momentum, or even both. Depending on the energy of the incoming electrons, different tunneling events are possible and since the conductance of the junction is proportional to the tunneling probability, we can measure the atomic states of the atom by measuring the differential conductance $\frac{dI}{dV}$.
To better understand this, let us take a look at figure 3.2. The $\frac{dI}{dV}$ is roughly constant up until approximately 1 mV. For bias voltages $>$ 1 mV, a sudden increase in differential conductance is measured. This corresponds to the opening of an extra tunneling channel, if the electrons have an energy $>$ $\mathrm{eV}_{threshold}$.

By using a spin-polarized tip, another feature appears in the $\frac{dI}{dV}$ measurement: the step size at the threshold voltage differs for positive and negative bias. The reason for this was described in section 3.4. We can make use of this to measure the degree of tip polarization.

4.3 Resonant driven transition in a 2 level system: The Rabi model

When an atom is placed in an alternating electric field, the atomic state will oscillate between unperturbed atomic states as a result of the atom-field interaction. In this section, we describe the driven transition occurring in a two level system according to the Rabi model [13].
We start of by defining the two atomic states as $|g\rangle$ and $|e\rangle$. Conventionally, $|g\rangle$ is the lowest of the two states. The two states have energies E_g and E_e respectively. The energy difference between the two states is given by $\Delta E = E_e - E_g$, to which is associated a characteristic frequency of $\omega_0 = \frac{\Delta E}{\hbar}$. To describe the atom-field interaction, we can write the following interaction Hamiltonian:

$$H^{(1)}(t) = V_0 \cos(\omega t) \tag{4.1}$$

where ω is the frequency of the driving electric field and V_0 is the amplitude of the driving field. Furthermore, we can write down the state vector of the system as:

$$|\Psi(t)\rangle = C_g(t)e^{-\frac{iE_g t}{\hbar}}|g\rangle + C_e(t)e^{-\frac{iE_e t}{\hbar}}|e\rangle \tag{4.2}$$

Substituting 4.1 and 4.2 in the Schrödinger equation, we get:

$$i\hbar\frac{d\Psi}{dt} = H\,\Psi(t)$$

$$i\hbar\left[\left(\dot{C}_g(t) + C_g(t)\left(\frac{-iE_g}{\hbar}\right)\right)e^{-\frac{iE_g t}{\hbar}}|g\rangle + \left(\dot{C}_e(t) + C_e(t)\left(\frac{-iE_e}{\hbar}\right)\right)e^{-\frac{iE_e t}{\hbar}}|e\rangle\right] = V_0\cos(\omega t)\left[C_g(t)e^{-\frac{iE_g t}{\hbar}}|g\rangle + C_e(t)e^{-\frac{iE_e t}{\hbar}}|e\rangle\right] + H_0\,\Psi$$

Now, taking the inner product with $\langle g|$ and $\langle e|$ respectively, we obtain 2 equations:

$$i\hbar\dot{C}_g(t)e^{-\frac{iE_g t}{\hbar}} = \cos(\omega t)C_e(t)e^{-\frac{iE_e t}{\hbar}}\langle g|V_0|e\rangle$$

$$i\hbar\dot{C}_e(t)e^{-\frac{iE_et}{\hbar}} = \cos(\omega t)C_g(t)e^{-\frac{iE_gt}{\hbar}}\langle e|V_0|g\rangle$$

Notice that $\langle g|V_0|g\rangle$ and $\langle e|V_0|e\rangle$ are 0, due to the quantum mechanical formulation of the electric field operator. Letting $\nu = \langle g|V_0|e\rangle = \langle e|V_0|g\rangle$, we get:

$$\dot{C}_g(t) = -\frac{i}{\hbar}\nu\cos(\omega t)C_e(t)e^{-\frac{i(E_e-E_g)t}{\hbar}} = -\frac{i}{\hbar}\nu\cos(\omega t)C_e(t)e^{-i\omega_0 t}$$

and

$$\dot{C}_e(t) = -\frac{i}{\hbar}\nu\cos(\omega t)C_g(t)e^{\frac{i(E_e-E_g)t}{\hbar}} = -\frac{i}{\hbar}\nu\cos(\omega t)C_g(t)e^{i\omega_0 t}$$

Writing $\cos(\omega t)$ as a complex number:

$$\dot{C}_g(t) = -\frac{i}{2\hbar}\nu C_e(t)\left(e^{i(\omega-\omega_0)t} + e^{-i(\omega+\omega_0)t}\right)$$
$$\dot{C}_e(t) = -\frac{i}{2\hbar}\nu C_g(t)\left(e^{i(\omega+\omega_0)t} + e^{i(\omega_0-\omega)t}\right)$$

Assuming that the frequency of the driving field is close to the resonance frequency, the $\omega + \omega_0$ term oscillates very rapidly, leaving the $\omega_0 - \omega$ term to dominate the expression. Therefore we can neglect the $\omega + \omega_0$ term. This is called the Rotating Wave Approximation. Defining the detuning as $\delta = \omega_0 - \omega$, we get:

$$\dot{C}_g(t) = -\frac{i}{2\hbar}\nu e^{-i\delta t}C_e(t) \tag{4.3}$$

$$\dot{C}_e(t) = -\frac{i}{2\hbar}\nu e^{i\delta t}C_g(t) \tag{4.4}$$

We shall now proceed to solve this system of coupled differential equations. Taking the time derivative of 4.4. we get:

$$\ddot{C}_e(t) = -\frac{i}{2\hbar}\nu\left(i\delta C_g(t) + \dot{C}_g(t)\right)e^{i\delta t}$$

Substituting 4.3 into this result, we find:

$$\ddot{C}_e(t) = -\frac{i}{2\hbar}\nu\left(i\delta C_g(t) + \left[-\frac{i}{2\hbar}\nu e^{-i\delta t}C_e(t)\right]\right)e^{i\delta t}$$
$$\ddot{C}_e(t) = -\left(\frac{\nu}{2\hbar}\right)^2 C_e(t) + \frac{\nu}{2\hbar}\delta e^{i\delta t}C_g(t)$$

Version of October 11, 2017– Created October 11, 2017 - 16:15

Rewriting 4.4 and inserting it in this result:

$$\ddot{C}_e(t) = -\left(\frac{\nu}{2\hbar}\right)^2 C_e(t) + \frac{\nu}{2\hbar}\delta e^{i\delta t}\left[\frac{2\hbar i}{\nu}e^{-i\delta t}\dot{C}_e(t)\right]$$

$$\ddot{C}_e(t) - i\delta\dot{C}_e(t) + \left(\frac{\nu}{2\hbar}\right)^2 C_e(t) = 0$$

As an Ansatz, we use:

$$C_e(t) = \sum_i c_i e^{\lambda_i t}, \quad c_i \in \mathbb{Z}$$

Substitution in the differential equation yields:

$$\lambda^2 - i\delta\lambda + \left(\frac{\nu}{2\hbar}\right)^2 = 0$$

$$\lambda_\pm = \frac{i}{2}\left(\delta \pm \sqrt{\delta^2 + \left(\frac{\nu}{\hbar}\right)^2}\right)$$

Let $\Omega = \sqrt{\delta^2 + \left(\frac{\nu}{\hbar}\right)^2}$:

$$\lambda_\pm = \frac{i}{2}(\delta \pm \Omega)$$

Finally, we find:

$$\begin{aligned} C_e(t) &= c_1 e^{\frac{i(\delta+\Omega)t}{2}} + c_2 e^{\frac{i(\delta-\Omega)t}{2}} \\ &= e^{\frac{i\delta t}{2}}(c_1 e^{\frac{i\Omega t}{2}} + c_2 e^{-\frac{i\Omega t}{2}}) \end{aligned}$$

and using 4.4:

$$\begin{aligned} C_g(t) &= \frac{2\hbar i}{\nu}e^{-i\delta t}\dot{C}_e(t) \\ &= \frac{2\hbar i}{\nu}e^{-i\delta t}\frac{\partial}{\partial t}\left[e^{\frac{i\delta t}{2}}(c_1 e^{\frac{i\Omega t}{2}} + c_2 e^{\frac{-i\Omega t}{2}})\right] \\ &= \frac{2\hbar i}{\nu}e^{-\frac{i\delta t}{2}}\left(i\frac{\delta}{2}(c_1 e^{\frac{i\Omega t}{2}} + c_2 e^{-\frac{i\Omega t}{2}}) + i\frac{\Omega}{2}(c_1 e^{\frac{i\Omega t}{2}} - c_2 e^{-\frac{i\Omega t}{2}})\right) \\ &= -\frac{\hbar}{\nu}e^{-\frac{i\delta t}{2}}\left(\delta(c_1 e^{\frac{i\Omega t}{2}} + c_2 e^{-\frac{i\Omega t}{2}}) + \Omega(c_1 e^{\frac{i\Omega t}{2}} - c_2 e^{-\frac{i\Omega t}{2}})\right) \end{aligned}$$

What is left to do now, is to choose proper initial conditions and calculate constants c_1 and c_2. As initial conditions, we assume that at $t = 0$, the levels are populated according to the Boltzmann distribution. This means that we can write:

$$\frac{C_e^2(0)}{C_g^2(0)} = \frac{e^{-\frac{E_e}{KbT}}}{e^{-\frac{E_g}{KbT}}} = e^{-\frac{\Delta E}{KbT}} \equiv B$$

Furthermore, normalization of the wavefunction requires that:

$$C_g^2(t) + C_e^2(t) = 1$$

If we now combine these criteria, we find for our initial conditions:

$$C_g(0) = \frac{1}{\sqrt{1+B}}$$
$$C_e(0) = \sqrt{\frac{B}{1+B}}$$

Setting $t = 0$ in the expressions obtained for $C_g(t)$ and $C_e(t)$, we get:

$$C_e(0) = c_1 + c_2 = \sqrt{\frac{B}{1+B}}$$
$$C_g(0) = -\frac{\hbar}{\nu}\left(\delta(c_1 + c_2) + \Omega(c_1 - c_2)\right) = \frac{1}{\sqrt{1+B}}$$

After doing some algebra, we can solve this system of coupled equations to get:

$$c_1 = -\frac{\sqrt{B}(\delta - \Omega) + \frac{\nu}{\hbar}}{2\Omega\sqrt{1+B}}$$
$$c_2 = \frac{\sqrt{B}(\delta^2 - \Omega^2) + \frac{\nu}{\hbar}(\delta - \Omega)}{2\Omega\sqrt{1+B}(\delta - \Omega)}$$

This means that we now have obtained a time dependent expression for the wavefunction of an atom in an oscillating electric field. To further illustrate the meaning of this model, we can plot the probability of finding the atom in state $|g\rangle$ or $|e\rangle$, i.e., $|C_g(t)|^2$ or $|C_e(t)|^2$. Below, several plots are generated for different input parameters. For now, we will not consider the effect of changing the amplitude of the applied electric field. We will solely vary the frequency of the applied field ($f = \frac{\omega}{2\pi}$), and the temperature of the atom:

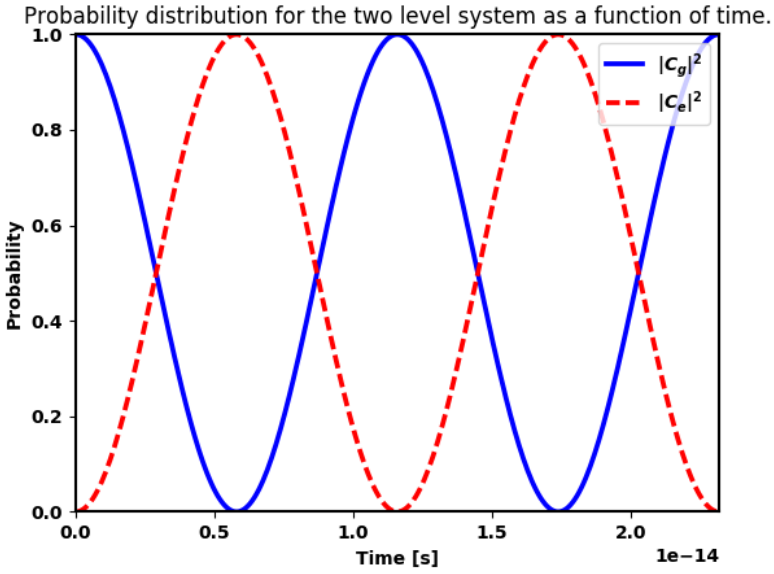

Figure 4.1: *Time evolution of the probabilities $|C_g(t)|^2$ and $|C_e(t)|^2$, associated with finding the atom in state $|g\rangle$ or $|e\rangle$ respectively. The plot was generated with the following input parameters: $\delta = 0$, $T = 0K$*

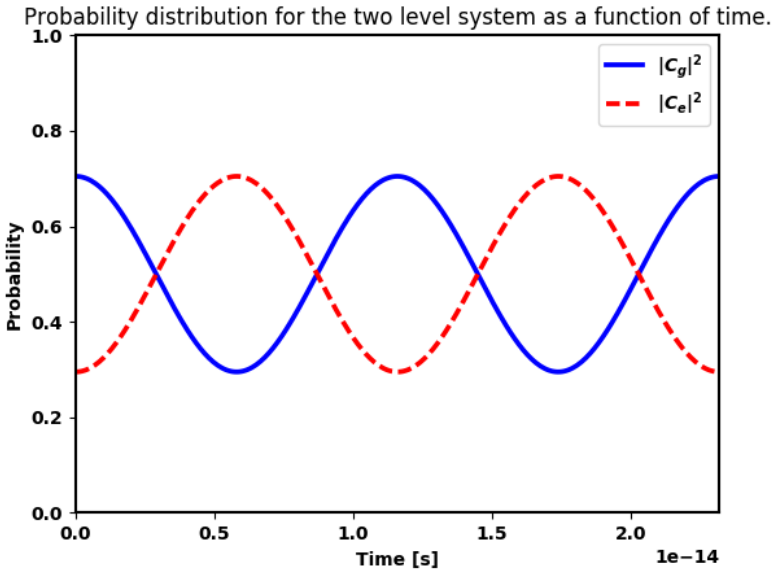

Figure 4.2: *Time evolution of the probabilities $|C_g(t)|^2$ and $|C_e(t)|^2$, associated with finding the atom in state $|g\rangle$ or $|e\rangle$ respectively. The plot was generated with the following input parameters: $\delta = 0$, $T = 2K$*

From the difference between figure 4.1 and 4.2, it becomes clear that finite temperature dampens the amplitude of the Rabi oscillation. This means that the Rabi oscillation itself becomes less defined, because the probability of finding the atom in a certain state never reaches one.
The effect of finite detuning becomes clear from the difference between figure 4.1, 4.3 and 4.4. Judging from these plots, the detuning becomes relevant when its magnitude is of the order of $\frac{\nu}{\hbar}$. This is expected, since we derived that $C_g(t)$ and $C_e(t)$ oscillate with $\Omega = \sqrt{\delta^2 + \left(\frac{\nu}{\hbar}\right)^2}$. In turn, we can also conclude from this that the effect of detuning on the oscillation frequency can be controlled by varying the amplitude of the applied electric field (ν). It should however be observed that knowing the exact amplitude of the electric field as felt by the adatom is almost impossible, since we generate this field inside a tunnel junction contained in the STM head. This is far from an ideal microwave cavity and hence there is a relatively large uncertainty in amplitude of the applied electric field. Due to the geometry of STM, the alternating electric field can only oscillate parallel to the junction unless we use some secondary antenna to generate an electric field. On the other hand, we describe above that for the combination of adatom and substrate of choice, the magnetic anisotropy axis points parallel to the sample surface. This means that in theory, for this combination it is impossible to drive the transition between two states due to orthogonality of the magnetic moment of the adatom and the amplitude of the driving field. In practice, however, one can hope that some microwave signal reflects non-trivially in the junction and still drives the transition. Furthermore, we are assuming here that the magnetic moment of the adatom in its ground state is polarized, parallel to the magnetic anisotropy axis. In practice, due to thermal fluctuation, the moment might deviate slightly from this, giving rise to another opportunity to drive the adatom with an RF field in the tunnel junction.

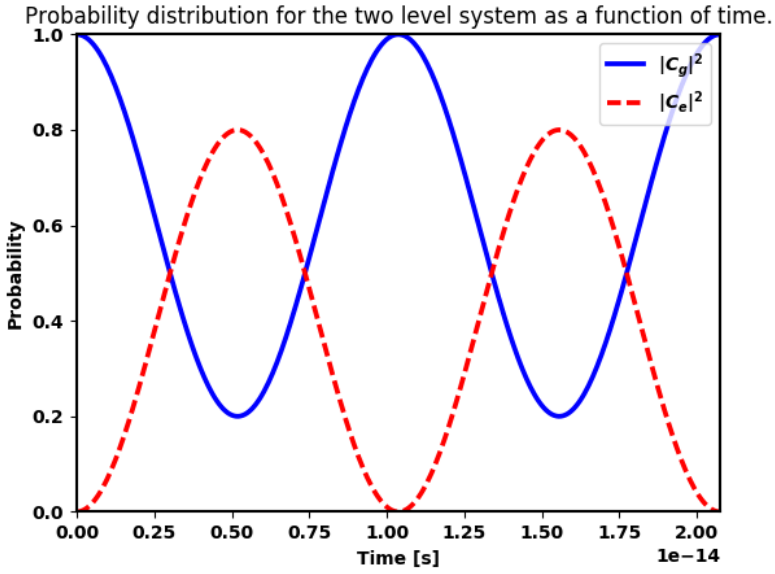

Figure 4.3: *Time evolution of the probabilities $|C_g(t)|^2$ and $|C_e(t)|^2$, associated with finding the atom in state $|g\rangle$ or $|e\rangle$ respectively. The plot was generated with the following input parameters: $\delta = 0.5\frac{\nu}{\hbar}$, $T = 0K$*

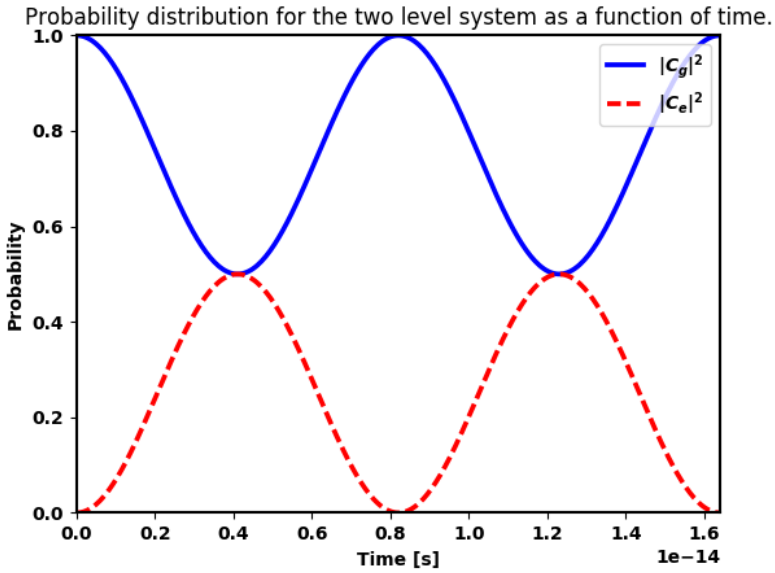

Figure 4.4: *Time evolution of the probabilities $|C_g(t)|^2$ and $|C_e(t)|^2$, associated with finding the atom in state $|g\rangle$ or $|e\rangle$ respectively. The plot was generated with the following input parameters: $\delta = \frac{\nu}{\hbar}$, $T = 0K$*

4.4 Big spin Hamiltonian

Upon placing a magnetic adatom on a substrate, the energy levels of the adatom are influenced by the magnetic environment of the substrate. Typically, this magnetic environment is not isotropic. To lowest order, we can describe this anisotropic environment by the so called big spin Hamiltonian:

$$H_S = -g\mu_b \mathbf{B} \cdot \mathbf{S} + DS_z^2 + E(S_x^2 + S_y^2) \tag{4.5}$$

Where μ_b is the Bohr magneton and D and E are the axial- and transverse magnetic anisotropy parameters.
Typically, the eigenstates of a Hamiltonian with a magnetic term are characterized by their magnetic quantum number (m), i.e. the magnitude of the z-projection of the spin angular momentum of the state. For the big spin Hamiltonian, this will also be the case, with the addition that besides the conventional Zeeman term, there is the axial anisotropy term which further divides the energies depending on the absolute value of m. Furthermore, the eigenstates of the big spin Hamiltonian will not be purely dependent on m, due to the transverse anisotropy term which mixes the eigenstates and a possible magnetic field component parallel to the magnetic easy axis.

4.5 Tunneling current in junction containing a magnetic adatom

When a magnetic adatom is placed in a tunnel junction, the tunneling current can be divided into three components. This was first derived by Fransson et al. [14], and also independently by Delgado et al. [15]. In this report, we will go over the derivation and use the result of Delgado et al., since the formulas presented in their paper are more compact and easier to interpret.
To derive the magnitude of the tunneling current, Delgado et al. solve the master equation for the eigenstates $|m\rangle$ of the Hamiltonian we presented in equation 4.5. Transitions between different eigenstates can occur due to exchange of spin angular momentum with delocalized electrons, i.e. tunneling electrons from the tip or sample. The occupation probability of a spin state $|m\rangle$, P_m should satisfy:

$$\frac{dP_m}{dt} = \sum_{m',\eta\eta'} P_{m'} W_{m',m}^{\eta'\to\eta} - P_m \sum_{m',\eta\eta'} W_{m,m'}^{\eta\to\eta'}$$

where $W_{m,m'}^{\eta\to\eta'}$ is the transition rate between state $|m\rangle$ and $|m'\rangle$ caused by quasiparticles which come from reservoir η and end up in reservoir η'. With reservoir, we mean either the tip or sample.
These scattering rates can be written as:

$$W_{m,m'}^{\eta\to\eta'} = \frac{\pi|T_s\nu_\eta\nu_{\eta'}|^2}{\hbar}G(\Delta_{m,m'}+\mu_\eta-\mu_{\eta'})\Sigma_{m,m'}^{\eta\eta'}$$

Where T_s is an element of the tunneling matrix, ν_i are dimensionless factors parametrizing the hopping integral between tip-adatom (ν_t) or sample-adatom (ν_s), $G(\omega)=\frac{\omega}{1-e^{-\frac{\omega}{KbT}}}$, are the phase factors associated with quasiparticle scattering, $\Delta_{m,m'}$ is the energy difference between state $|m'\rangle$ and $|m\rangle$, μ_i is the chemical potential associated with the electrode i and $\Sigma_{m,m'}^{\eta\eta'}$ are spin matrix elements:

$$2\Sigma_{m,m'}^{\eta\eta'} = |S_z^{m,m'}|^2(\rho_{\eta\uparrow}\rho_{\eta'\uparrow}+\rho_{\eta\downarrow}\rho_{\eta'\downarrow})+|S_+^{m,m'}|^2\rho_{\eta\downarrow}\rho_{\eta'\uparrow}+|S_-^{m,m'}|^2\rho_{\eta\uparrow}\rho_{\eta'\downarrow}$$

where $S_j^{m,m'}=\langle m|S_j|m'\rangle$ and $\rho_{\eta,\sigma}$ is the density of states at the Fermi energy of electrons with spin σ in electrode η. In this equation, it also becomes apparent that a spin-polarized tip (or even a spin-polarized sample for that matter) creates an imbalance in the different transition rates.
Further evaluation of the individual transition rates results in a tunneling current, that can be divided in three components:

$$I = I_0 + I_{mr} + I_{in}$$

Here, I_0 is an elastic component of the tunneling current and is independent of the polarization of the tip and sample. I_{mr} is also elastic but it depends on the relative spin polarization between the tip and adatom. I_{in} is an inelastic component and it also depends on the spin polarization of the adatom. The individual current components can be expressed as:

$$I_0 + I_{mr} = -\frac{2}{e}G_0\left(1+x\langle S_z\rangle P_t\right)i_-(-eV) \tag{4.6}$$

and

$$I_{in} = -\frac{G_S}{e}\sum_{m,m'}\left[i_-(\Delta_{m,m'}-eV)\sum_j|S_j^{m,m'}|^2+P_t i_+(\Delta_{m,m'}-eV)\Im(S_x^{m,m'}S_y^{m',m})\right]P_m(V) \tag{4.7}$$

In these equations, $G_0 \equiv \frac{e^2\pi\rho_t\rho_s}{4\hbar}|T_0\nu_t\nu_s|^2$ is the elastic junction conductance, $Gs = x^2G_0$ is the inelastic conductance, where $x = \frac{T_s}{T_0}$ is the relative intensity difference of the inelastic- to the elastic channel.
Furthermore, $P_t = \frac{\rho_{t\uparrow}-\rho_{t\downarrow}}{\rho_{t\uparrow}+\rho_{t\downarrow}}$ is the tip polarization is the z- direction, $i_\pm(\Delta_{m,m'} - eV) = G(\Delta_{m,m'} - eV) \pm G(\Delta_{m,m'} + eV)$ and $\langle S_z\rangle = \sum_m P_m(V)\langle m|S_z|m\rangle = \langle\Psi|S_z|\Psi\rangle$ is the average spin polarization along the z-direction of the magnetic adatom.
Note that equation 4.6 is not entirely identical to the result in the paper, since we suspect a typo in the paper. From dimensional analysis, the equation given here should be correct and thus this expression was also used in the simulations (chapter 5).
In case we decide to drive the adatom with an applied alternating electric field, the state of the adatom will oscillate between what we consider its ground state and an excited state. This means that $\langle S_z\rangle$, which is of course dependent on the current state of the adatom, will also become a function of time and the magneto-resistive component of the tunneling current will become an alternating current which we could possibly measure using an impedance matching circuit. Nevertheless, this view of the oscillating system will only be valid if the DC bias voltage is set below the energy required to excite the spin state through inelastic scattering. If this is the case, the atom can only go in the excited state through the Rabi oscillations and the Rabi oscillations in itself should stay unperturbed. If the bias exceeds this limit, the atom can be excited through an inelastic tunneling process and it is unsure what effect this will have on the driven system. Since the transition is separated by an energy difference of $\Delta E \sim 100\mu$eV, this means that the bias voltage should be accurate in μV range.

Chapter 5

Simulated EPR data

In order to be able to comment on the feasibility of the experiments mentioned above, we wrote a Python code based on a theoretical result of Delgado et al. [15] (section 4.5) that calculates the tunneling current when driving the magnetic adatom with an alternating electric field. This code can be modified to estimate results for the T_1 time measurement and for the DC EPR measurements conducted by Baumann et al. [3], but due to a shortage of time, this will have to be done in a future project (see Future research).
To describe the tunneling current as measured in a junction containing a Rabi precessing atom, we assume a model based on sections 4.3 and 4.5. The atom is assumed to be unperturbed by the tunneling electrons, which is valid for small bias voltage (e $V_{bias} < \Delta E$). We calculate the energies and eigenstates for iron atoms on CuN according to section 4.4. The atom is assumed to oscillate between its two lowest lying energy states. We calculate equation 4.6, since this contains the AC current component due to time dependent magneto resistance of the tunnel junction. To clarify: When the atom oscillates between two states with different $\langle S_z \rangle$, the magneto resistance of the total junction becomes a function of time since the projection of the atom spin component on the tip polarization axis varies with time. Hence an alternating current component can be measured with a spin polarized tip.
It should be mentioned that the calculations done in this chapter are not fully representative of experimental reality, since there is no way to accurately estimate all the physical parameters of the problem. Especially estimating the amplitude of the driving electric field is not an easy task, since as we mentioned before, a tunnel junction in a STM head is far from an ideal microwave cavity. This is quite problematic for the viability of

our calculations since in section 4.3, it was shown that the amplitude of the driving field determines the Rabi oscillation frequency which is an important parameter because it determines how we need to tune our RF- circuitry. Nevertheless, we proceeded to execute the Python code with what we consider to be realistic input parameters.
To start, we assume to be able to create an experimental environment similar to the conditions used in Baumann et al [3]. This means that we try to create a system Rabi oscillating between two levels split by a gap of roughly 100μeV, but this time with Fe atoms on CuN. Luckily, at zero applied magnetic field, the level splitting between the two lowest energy levels already equals 181μeV. This means that in that regard, we do not require much field parallel to the anisotropy axis, which is parallel to the sample (N- direction) and this condition is therefore favorable to us. To calculate the energies and eigenstates, we diagonalise the Big spin Hamiltonian of section 4.4 with parameters measured by Hirjibehedin et al [6].
At zero applied magnetic field, we find the energy spectrum of figure 5.1 and corresponding eigenstates:

$$\Psi_0 = 0.697300362563|2\rangle - 0.165965082889|0\rangle + 0.697300362563|-2\rangle$$
$$\Psi_1 = 0.707106781187|2\rangle - 1.36222468205e-15|0\rangle - 0.707106781187|-2\rangle$$
$$\Psi_2 = 0.707106781187|1\rangle - 0.707106781187|-1\rangle$$
$$\Psi_3 = 0.707106781187|1\rangle + 0.707106781187|-1\rangle$$
$$\Psi_4 = 0.117355035551|2\rangle + 0.986131629785|0\rangle + 0.117355035551|-2\rangle$$

Here, the z- axis , i.e. the quantization axis, was chosen parallel to the magnetic easy axis (parallel to the sample). This result fully matches the states predicted by Hirjibehedin et al [6]. It is clear that the lowest two states are mainly superpositions of $|2\rangle$ and $|-2\rangle$. In this case, the difference between the two states would be undetectable in IETS since $\langle S_z\rangle$ is roughly the same for both states, which is ~ 0.
If we start driving the transition between Ψ_0 and Ψ_1, we can write down the wavefunction of the adatom as: (equation 4.2)

$$|\Psi(t)\rangle = C_g(t)e^{-\frac{iE_gt}{\hbar}}|\Psi_0\rangle + C_e(t)e^{-\frac{iE_et}{\hbar}}|\Psi_1\rangle$$

Calculating $\langle S_z(t)\rangle = \langle\Psi(t)|S_z|\Psi(t)\rangle$ allows us to calculate the tunneling current (equation 4.6). As physical parameters, we estimate:

Version of October 11, 2017– Created October 11, 2017 - 16:15

Physical quantity	value	comment
Applied magnetic field	$0T$	-
Sample tilt angle	$0°$	-
Temperature	$2K$	-
Junction resistance	$100M\Omega$	-
Bias voltage	$0.1mV$	-
Magnetic moment of the adatom	$2.2\mu_b$	Magnetic moment of an individual iron atom
Electric field amplitude	$1 \times 10^5 V/m$	Assuming a parallel plate capacitor with a junction size of $1nm$ and $V_{rf} = 0.1mV$
Frequency of driving field	-	The detuning is set to 0.

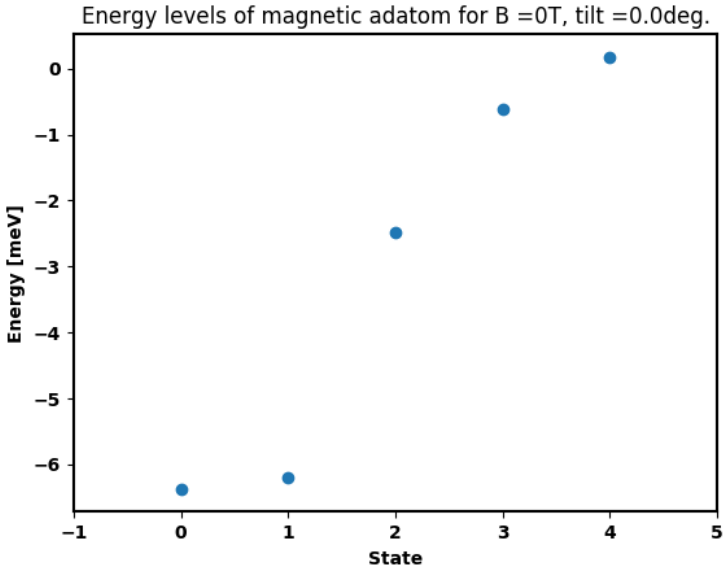

Figure 5.1: *Energy distribution of adatom states for Fe on CuN. The magnetic field is applied perpendicular to the sample and the tilt angle is measured between the current N-direction axis and the N-direction axis without sample tilt.*

With the parameters given above, calculating the tunneling current with the Python code results in figure 5.3 and 5.4.

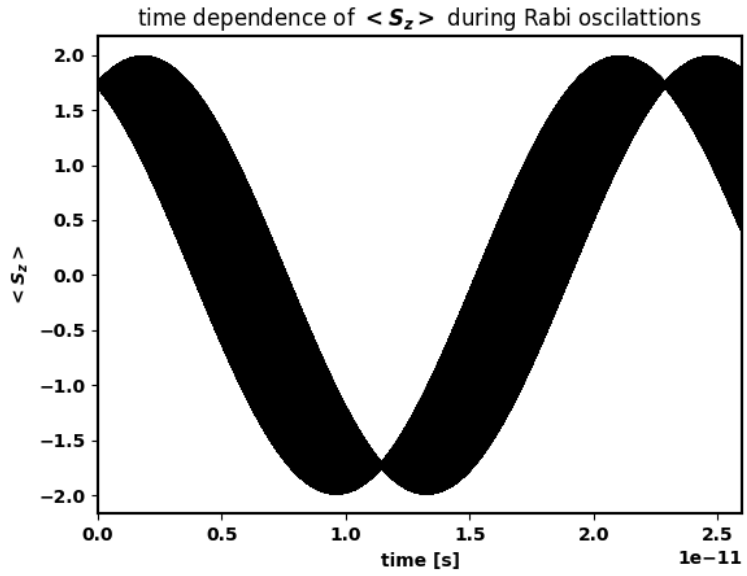

Figure 5.2: *Expectation value for the z- component of the spin angular momentum of the magnetic adatom undergoing Rabi oscillations according to the table presented above.*

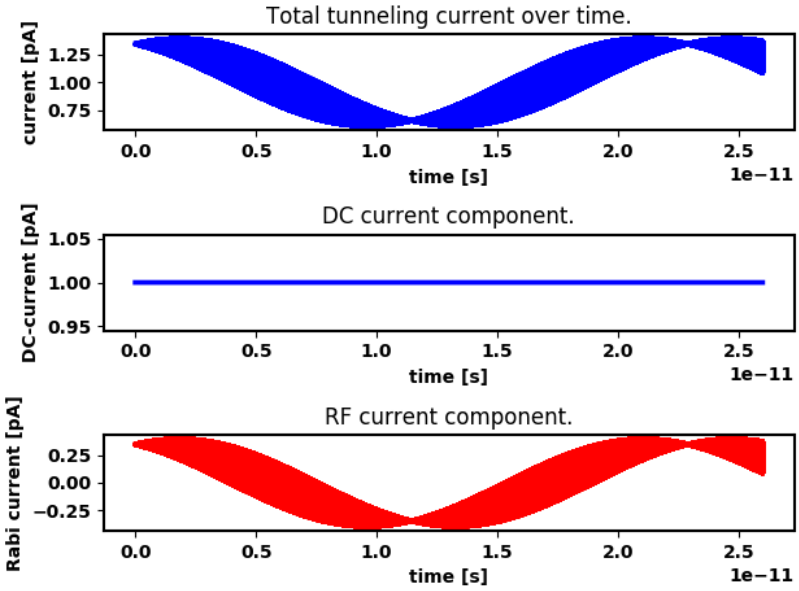

Figure 5.3: *Simulated tunneling current measured with a magnetic adatom in the tunnel junction undergoing Rabi oscillations.*

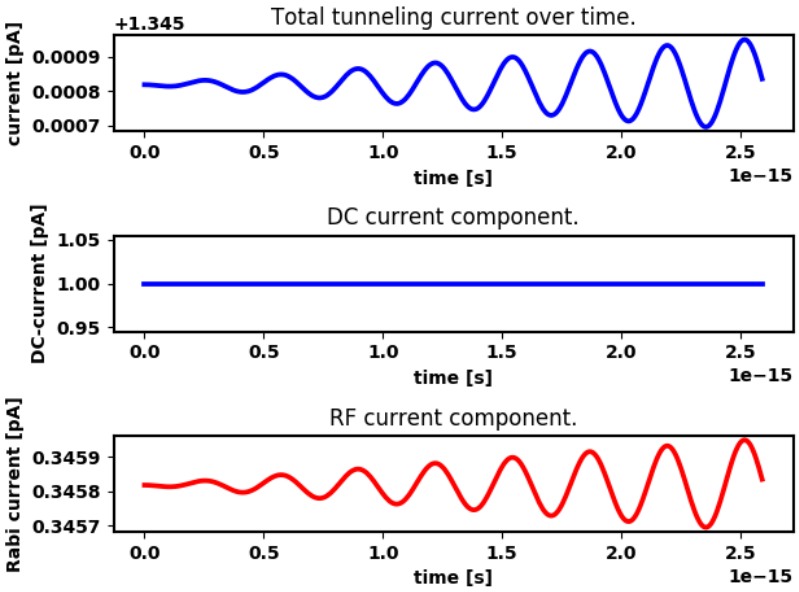

Figure 5.4: *Zoom in of tunneling current presented in figure 4.3. By zoomin ing, it becomes apparent that besides the main oscillation on timescales of* $\sim 25ps$*, there is a secondary oscillation on much shorter timescales (*$\sim 0.5fs$*).*

With a Rabi precessing atom in the tunnel junction, for the parameters we declared above, the tunnel current is modulated at two frequencies. The major oscillation happens at timescales of ∼ps, corresponding to an AC current component in THz range. Furthermore, upon closer inspection (fig 5.4), we see that there is a second modulation at much shorter timescales ($\sim fs$). It is actually this second oscillation that corresponds to the Rabi frequency, which is in this case $\frac{\Omega}{2\pi} = 3.08 \times 10^{15}$ Hz. The first oscillation is due to the $e^{-\frac{iE_i t}{\hbar}}$ term in the wavefunction, for which in both cases $\frac{E_e}{h} = \frac{E_g}{h} \approx 1.5 \times 10^{12}$ Hz.
Measuring the contribution to the tunneling current in real time of both these oscillations will be extremely difficult due to their very high frequencies. To solve this, lowering the Rabi frequency seems a logical step. However, as determined previously, the Rabi frequency is proportional to the amplitude of the applied driving electric field. This is approximately given by $|E_{drive}| = \frac{V_{rf}}{d_{junction}}$, if we assume a parallel plate capacitor model. In this formula, V_{rf} is the applied RF- voltage on the junction (rms), and $d_{junction}$ is the distance between tip and sample. Due to the fact that our samples are insulating (due to the CuN layer), $d_{junction}$ is limited because the junction resistance will quickly become too large. This, in addition to

the fact that the DC bias is limited by the level splitting between the two levels in order to refrain from perturbing the Rabi oscillations, makes that $d_{junction}$ is not a very flexible variable. The sole parameter left to tune is then V_{rf}. Naïvely one could think that this value can be made arbitrarily small, provided that one cannot go lower than the noise limit of the device used to create the RF bias. However, the second factor one has to take into account is the transfer function of the cable connecting the STM head to room temperature devices. As discussed previously, associated with this cable is a parasitic capacitance which low-pass filters any signals going through. The accuracy with which we can determine the transfer function of this cable, together with the noise of the RF device determines the lower limit to V_{rf}.
Tuning the magnetic field does not influence the Rabi frequency. Consequently, it does not make any sense at this point to rerun the simulation for different magnetic field values, since the frequency of the signal generated by Rabi precession is just too large to detect. With this, we therefore conclude this investigation on EPR measurements on a single spin device.

Chapter 6

Future research

6.1 Outlook

Because of short time constraints, this research if far from complete. To continue this project, the following topics should be considered:

- **Further parameter space exploration using the python code in order to create an optimal experiment:** In chapter four, the main focus was to simulate EPR measurements using individual Fe atoms on CuN. With minor modifications, the existing python code (appendix A.1) can be used to also describe measurements on single atom systems without a driving field. This might be useful, since we think that measuring relaxation times, especially T_1, is a lot easier than measuring Rabi precession (section 6.2).

- **Theoretical model check: Big spin Hamiltonian.** To calculate the energies and eigenstates of the magnetic adatom in the tunnel junction, the python code solves the Schrödinger equation for the so called big spin Hamiltonian presented in section 4.4. Even though this is confirmed to be a valid model [4], in some instances, for example reference [3], a more advanced model called the Ligand field Hamiltonian is used. We think it is interesting to see how these different models compare to each other.

- **Theoretical model check: Rabi Precession.** In section 4.3, we describe a way to model an atom inside an oscillating electric field based on reference [13]. It might be useful to also use a more general theoretical framework, starting from the Bloch equations and comparing the outcome to the results we obtained in this report.

- **Temperature effects:** In our python simulation, temperature only enters in the initial conditions of the population degree of the two level system. It should be checked if this is done correctly and probably the effect of level broadening should also be researched in the context of Rabi oscillations.

- **STM characterization.** As mentioned in chapter 5, to properly simulate the effects of a Rabi oscillating atom in the tunnel junction, it is invaluable to know the exact amplitude of the applied electric field. Hence, should we want to further investigate EPR measurement possibilities, measuring the transfer function of our STM is a step in the right direction. This might be good in general, for future RF- STM experiments. We can also think about building an antenna close to the tunnel junction in order to generate the AC electric field with a secondary electrode.

6.2 Final thoughts

In the end, I am personally most confident about time resolved T_1 measurements of Fe-Cu dimers on CuN since we know what we are supposed to measure (Loth et al.[2]: $T_1 \sim 100ns$) and it seems doable with only minor modifications of our current RF- circuitry. It will still be challenging because we need to install the magnet, need to learn to grow CuN samples, etc., but it is also for this reason that I think it is good to start here in order to learn these skills. Once we can successfully do this, we can think about doing the more complicated EPR measurements, should we find that they are useful to do. After all, even though I think it is interesting to measure real time Rabi precession, the question is what we can learn from it in terms of new physics and knowledge for future research projects like spin fluctuation measurements in superconductors.

Version of October 11, 2017– Created October 11, 2017 - 16:15

Appendices

Appendix A

Python code

A.1 EPR measurement simulation

This python code was used to simulate the data presented in chapter 4. It can be modified to also simulate DC current measurements on a magnetic adatom in the tunnel junction.
This code also contains the possibility to export the generated data to .npz files, which can be loaded with the code presented in A.2 in order to do a Fourier transform on it for easy data analysis.

```
#Simulation: magnetic adatom in tunnel junction

import numpy as np
from matplotlib import pyplot as plt

import os # these modules are used to export the simulated current data
import errno


plt.close('all')

#plot graphics:
plt.rcParams["font.weight"] = 'bold'
plt.rcParams["axes.labelweight"] = 'bold'
plt.rcParams['lines.linewidth'] = 2.7
plt.rcParams['axes.linewidth'] = 1.5

#constants:

Mub = 5.7883818012e-5 #bohr magneton (eV/T)
h = 4.135667662e-15 #eV*s
```

```
hbar = 1.054571800e-34 #J*s/rad
kb = 8.6173303e-5 #ev/K
e = 1.60217662e-19 #C

#########################################################################
#create spin algebra:
class spin:
    def __init__(self):
        Su = np.array([[0,2,0,0,0],[0,0,np.sqrt(6),0,0],\
                       [0,0,0,np.sqrt(6),0], \
                       [0,0,0,0,2],[0,0,0,0,0]])
        Sd = np.array([[0,0,0,0,0],[2,0,0,0,0],\
                       [0,np.sqrt(6),0,0,0], \
                       [0,0,np.sqrt(6),0,0],[0,0,0,2,0]])

        self.x = (Su +Sd)/2
        self.y = (Su -Sd)/2j
        self.z = np.array([[2,0,0,0,0],[0,1,0,0,0],[0,0,0,0,0], \
                   [0,0,0,-1,0],[0,0,0,0,-2]])

S = spin()
#########################################################################

#functions:
def spinHamiltonian(g,B,D,E):

    H = -1*g*Mub*(B[0]*S.x+B[1]*S.y+B[2]*S.z) +\
                 D*np.linalg.matrix_power(S.z,2) + \
                 E*(np.linalg.matrix_power(S.x,2) - \
                    np.linalg.matrix_power(S.y,2)) #note that here,
                 #there's a minus sign for the Zeeman term,
                 #contrary to Hirjibehedin.

    E,States = np.linalg.eig(H)

    '''
    #check if energies are real valued:
    if np.size(np.nonzero(E.imag)) >= 1:
        print('Error: Energies contain imaginary values.')
    '''
    #sort energies & states:
    order = E.argsort()
    E = E[order]
    States = States[:,order]

    return States,E.real

def state(s):
    lib = ['|2>','|1>','|0>','|-1>','|-2>']
```

```
71
72      string = ''
73      for i in range(len(s)):
74          if s[i] == 0:
75              string = string
76          else:
77              if s[i].imag == 0:
78                  if s[i].real < 0:
79                      string = string[:-2]
80                      string = string + ' ' + str(s[i].real) +lib[i] + '+ '
81                  else:
82                      string = string + str(s[i].real) +lib[i] + '+ '
83              else:
84                  string = string + str(s[i]) +lib[i] + '+ '
85
86
87      return string[:-2]
88
89  def visualoutput_adatomstates(init,E,S,B,theta):
90      if init == True:
91          #plot energy spectrum:
92          fig1 = plt.figure()
93          ax1 = fig1.add_subplot(111)
94          ax1.scatter(range(len(E)),E*1e3)
95          ax1.set_xlabel('State')
96          ax1.set_ylabel('Energy [meV]')
97          ax1.set_xlim([-1,len(E)])
98          title = 'Energy levels of magnetic adatom for B ='+ str(B) +\
99          'T, tilt ='+ str(theta*180/np.pi) +'deg.'
100         ax1.set_title(title)
101
102         #determine useful parameters:
103         delta_E = E[1] - E[0]
104         f0 = delta_E/h
105
106         print('')
107         print('-------------------------------------------------------------')
108         print('levelsplit = ', delta_E*1e3, 'meV')
109         print('f0 = ', f0*1e-9, 'GHz')
110         print('')
111
112         print('Eigenstates:')
113         for i in range(len(S[0,:])):
114             print('V' + str(i) + ' = ' + state(S[:,i]), '\n')
115         print('-------------------------------------------------------------')
116
117 def expecval(s1,s2,A):
118     #calculate expectationvalue of operator A given states s1,s2
119     inprod = np.dot(A,s2)
```

```
120     inprod = np.vdot(s1,inprod)
121
122     return inprod
123
124 def expectations(State,visual):
125     #calculates expectation values for the time-independent states of the
126     #Hamiltonian, without driving field
127
128
129     #calculate expectation value:
130     Sx2 = np.zeros(len(State[0,:]))
131     Sy2 = np.zeros(len(State[0,:]))
132     Sz = np.zeros(len(State[0,:]))
133
134     for i in range(len(State[0,:])):
135         Sz[i] = expecval(State[:,i],State[:,i],S.z)
136
137         Sx2[i] = expecval(State[:,i],State[:,i],\
138            np.linalg.matrix_power(S.x,2))
139         Sy2[i] = expecval(State[:,i],State[:,i],\
140            np.linalg.matrix_power(S.y,2))
141
142     if visual:
143         fig2 = plt.figure()
144
145         ax2 = fig2.add_subplot(311)
146         ax3 = fig2.add_subplot(312)
147         ax4 = fig2.add_subplot(313)
148         ax2.scatter(range(len(Sz)),Sz)
149         ax3.scatter(range(len(Sx2)),Sx2)
150         ax4.scatter(range(len(Sy2)),Sy2)
151
152
153         ax2.set_xlabel('statenr.')
154         ax2.set_ylabel('<Sz>')
155         ax2.set_title('Spin z-projection')
156         ax2.set_ylim([np.min(Sz) - 0.5*np.abs(np.min(Sz)),np.max(Sz) +\
157                       0.5*np.abs(np.max(Sz))])
158
159         ax3.set_xlabel('statenr.')
160         ax3.set_ylabel('<Sx^2>')
161         ax3.set_title('Spin x-projection')
162         ax3.set_ylim([0,5])
163
164         ax4.set_xlabel('statenr.')
165         ax4.set_ylabel('<Sy^2>')
166         ax4.set_title('Spin y-projection')
167         ax4.set_ylim([0,5])
168         fig2.tight_layout()
```

```
169
170     return Sz,Sx2,Sy2
171
172 def expec_t(state):
173     Sz = np.zeros(len(state[0,:]),dtype=complex)
174
175     for i in range(len(Sz)):
176         Sz[i] = expecval(state[:,i],state[:,i],S.z)
177
178     return Sz
179
180 def calc_tunnelcurrent(G0,x,P,V,Sz):
181
182     #Formula from Delgado et al. (PRL 104, 026601 (2010))
183     #(with correction and removal of factor 2)
184     I0 = G0*V
185     Img = G0*x* Sz * P*V
186
187     return I0,Img.real
188
189 def Rabi_state(State,Energy,Mu,E,f_drive,T,time,show_popgraph):
190     delta_E = Energy[1] - Energy[0]
191     f0 = delta_E/h
192
193     if f_drive == -1:
194         f_drive = f0
195
196
197     #Calculate boltzmann factor:
198     B = np.exp(-1*delta_E/(kb*T))
199
200
201     V = Mu*E
202     delta_w = 2*np.pi * (f0 - f_drive)
203     f_rabi = np.sqrt(delta_w**2 + (V/hbar)**2)
204
205     if type(time) == int:
206         t = np.linspace(0,time*2*np.pi/(f_rabi/2),100*time)
207     else:
208         t = time
209
210     #coefficient constants:
211     c1 = -1 * (np.sqrt(B)*(delta_w - f_rabi) + V/hbar)/(2*f_rabi*np.sqrt(1+B))
212     c2 = (np.sqrt(B)*(delta_w**2 - f_rabi**2) + (V/hbar)*(delta_w - f_rabi))\
213          /(2*f_rabi*np.sqrt(1+B)*(delta_w - f_rabi))
214
215     #wavefunction coefficients:
216     cg = -1 * (hbar/V) * np.exp(-1j*delta_w*t/2) * \
217               ((delta_w + f_rabi)*c1*np.exp(1j*f_rabi*t/2) \
```

```
                + (delta_w - f_rabi)*c2*np.exp(-1j*f_rabi*t/2))

    ce = np.exp(1j*delta_w*t/2)*(c1*np.exp(1j*f_rabi*t/2) + \
                c2*np.exp(-1j*f_rabi*t/2))

    if show_popgraph:
        fig_test = plt.figure()
        ax_test = fig_test.add_subplot(111)
        ax_test.plot(t,np.abs(cg)**2,'b-')
        ax_test.plot(t,np.abs(ce)**2,'r--')
        ax_test.set_xlabel('time [s]')
        ax_test.set_ylabel('Probability')
        ax_test.legend(['$P_g(t)$','$P_e(t)$'],loc='upper right')
        ax_test.set_title(\
        'Rabi oscillations between ground and first excited state')


    cg_tot = cg*np.exp(-2j*np.pi*Energy[0]*t/h)
    ce_tot = ce*np.exp(-2j*np.pi*Energy[1]*t/h)

    wavefunc = np.outer(State[:,0],cg_tot) + np.outer(State[:,1],ce_tot)

    return wavefunc,cg,ce,t



##########################################################################
#DEFINE INPUT HERE:
##########################################################################


B = 0 #applied magnetic field [T]
theta = 0 #tilt angle of the sample (angle between N-row in CuN and
#sampleholder [deg.])
T = 2 #temperature in K

G0 = 1/100e6 #junction elastic resistance(approx junction resistance)
Vbias = 1e-4

Mu = 2.2*Mub*e #magnetic moment of adatom (j/T)
E_applied = 1e5 #electri field amplitude (V/m)
f_drive = -1 #frequency of driving field (Hz), set to -1 if equal to
#resonance frequency


t = 20000#2000 #integer for nr of rabi oscillation periods, or
#array to define manually
Display_states = True
show_popgraph = False #toggle graphic display of population
```

```
#of states over time

export_data = False
filename = 'simulated_current/Rabidata_t=' + str(t) + '.npz'


#######################################################################
#Main program:
#######################################################################


theta = theta*np.pi/180 #convert angle to radians
State,E = spinHamiltonian(2.11,np.array([0,B*np.sin(theta-(np.pi/2)),\
                                         -1*B*np.cos(theta-(np.pi/2))]),\
    -1.55e-3,0.31e-3)


#print stuff to screen
print('')
print('Values calculated for input:')
print('B = ' , B , 'T')
print('theta = ' , theta*180/np.pi , 'degrees')
print('T = ', T , 'K')
print('\n')
print('Vbias = ' , Vbias*1e3 , 'mV')
print('Junction Resistance = ' , 1e-6/G0, 'Mohm')
print('Mu = ', Mu/(Mub*e) , 'Bohrmagnetons.')
print('Applied electric field amplitude = ' , E_applied , 'V/m')

if f_drive == -1:
    print('Applied field is in resonance with level spillting')
else:
    print('Driving frequency of field = ' , f_drive , 'Hz')

visualoutput_adatomstates(Display_states,E,State,B,theta)

wavefunc,cg,ce,t = Rabi_state(State,E,Mu,E_applied,f_drive,T,t,show_popgraph)




Sz = expec_t(wavefunc)

#debug:
fig_sz = plt.figure()
ax_sz = fig_sz.add_subplot(111)
#ax_sz.scatter(t,Sz,c=range(len(Sz)),cmap='gist_rainbow')
ax_sz.plot(t,Sz,'k-')
ax_sz.set_title('time dependence of $< S_z >$ during Rabi oscilattions')
```

```
316 ax_sz.set_xlabel('time [s]')
317 ax_sz.set_ylabel('< $S_z$ >')
318 ax_sz.set_xlim([t[0],t[-1]])
319
320
321
322
323
324
325 I0,Img = calc_tunnelcurrent(G0,1,0.2,Vbias,Sz)
326
327 fig_I = plt.figure();
328
329 ax_I1 = fig_I.add_subplot(411)
330 ax_I2 = fig_I.add_subplot(412)
331 ax_I3 = fig_I.add_subplot(413)
332 ax_I4 = fig_I.add_subplot(414)
333
334 ax_I1.plot(t,(I0+Img)*1e12,'b-')
335 ax_I1.set_xlabel('time [s]')
336 ax_I1.set_ylabel('current [pA]')
337 ax_I1.set_title('Total tunneling current over time.')
338
339 ax_I2.plot(t,I0*1e12*np.ones(len(t)),'b-')
340 ax_I2.plot(t,(I0 + Img)*1e12,'r-')
341 ax_I2.set_xlabel('time [s]')
342 ax_I2.set_ylabel('current [pA]')
343 ax_I2.set_title('Components of tunneling current over time.')
344
345 ax_I3.plot(t,I0*1e12*np.ones(len(t)),'b-')
346 ax_I3.set_xlabel('time [s]')
347 ax_I3.set_ylabel('DC-current [pA]')
348 ax_I3.set_title('DC tunneling component.')
349
350 ax_I4.plot(t,(Img)*1e12,'r-')
351 ax_I4.set_xlabel('time [s]')
352 ax_I4.set_ylabel('Rabi current [pA]')
353 ax_I4.set_title('Rabi tunneling component.')
354
355 fig_I.tight_layout()
356
357
358 if export_data:
359     #if path doesn't exist, create it:
360     print('Data exportation initialized.')
361     if not os.path.exists(os.path.dirname(filename)):
362         try:
363             os.makedirs(os.path.dirname(filename))
364         except OSError as exc:
```

```
365             if exc.errno != errno.EEXIST:
366                 raise
367
368     np.savez(filename, time = t, I0 = I0, Img = Img)
369     print('Data exportation completed.')
370
371
372 ########################################################################
373 #debug: check if data is saved succesfully:
374 debug_checkdata = False
375
376 if debug_checkdata:
377     data = np.load(filename)
378
379     if all(data['time'] == t) and data['I0'] == I0 and \
380           all(data['Img'] == Img):
381         print('Data exportation succesfull with 0 errors.')
382     else:
383         print('Error with data exportation!!!')
384 ########################################################################
```

A.2 Analysis code

This code was in the end not used in this report. It Fourier transform any exported data from the code in section A.1. It is therefor included for analysis purposes.

```
1  #script to do simulation analysis for the magenetic adatom in junction system
2
3  import numpy as np
4  from matplotlib import pyplot as plt
5
6
7  #plot graphics:
8  plt.rcParams["font.weight"] = 'bold'
9  plt.rcParams["axes.labelweight"] = 'bold'
10 plt.rcParams['lines.linewidth'] = 2.7
11 plt.rcParams['axes.linewidth'] = 1.5
12
13 def fourier(A,t):
14     samplespaceing = t[1] - t[0]
15
16     A_freq = np.fft.fft(A,norm='ortho')
17     f = np.fft.fftfreq(np.size(t), d=samplespaceing)
18
```

```
19      #order the arrays:
20      order = f.argsort()
21      f = f[order]
22      A_freq = A_freq[order]
23
24      return A_freq,f
25
26  def find_max(A,thresh):
27      #function returns arguments of local maxima of positive valued
28      #array (requires numpy module)
29
30      ls = np.empty(0,dtype=int)
31
32      #set boundary value to find maxima only above this threshold
33      if thresh:
34          lim = np.average(A)
35      else:
36          lim = 0
37
38      for i in np.arange(1,len(A)-1,1):
39          if A[i] >= A[i-1] and A[i] >= A[i+1] and A[i] > lim:
40              ls = np.append(ls,int(i))
41
42      return ls
43
44  ######################################################################
45  ######################################################################
46  ######################################################################
47
48  filename = 'simulated_current/Rabidata_t=50000.npz'
49
50
51  data = np.load(filename)
52
53  I0 = data['I0']
54  Img = data['Img']
55  t = data['time']
56
57
58  #fourier transforming the current:
59  I_f,frq = fourier(I0 + Img,t)
60  lmax = find_max(np.abs(I_f),True) #indices or large frequency peaks
61
62
63  plt.close('all')
64
65  fig_signal = plt.figure()
66  ax_t = fig_signal.add_subplot(221)
67  ax_f = fig_signal.add_subplot(222)
```

```
68  ax_lowf = fig_signal.add_subplot(223)
69  ax_hf = fig_signal.add_subplot(224)
70
71  if np.size(t) > 1000000:
72      #to prevent matplotlib crash, only plot portion of t-spectrum
73      ax_t.plot(t[0:1000000],(I0+Img[0:1000000])*1e12,'b-')
74      ax_t.set_xlabel('time [s]')
75      ax_t.set_ylabel('Current [pA]')
76      ax_t.set_title('Time dependent tunneling current.')
77  else:
78      ax_t.plot(t,(I0+Img)*1e12,'b-')
79      ax_t.set_xlabel('time [s]')
80      ax_t.set_ylabel('Current [pA]')
81      ax_t.set_title('Time dependent tunneling current.')
82
83  ax_f.plot(frq*1e-12,np.abs(I_f)*1e8,'b-')
84  ax_f.scatter(frq[lmax]*1e-12,np.abs(I_f[lmax])*1e8,marker='.',c='r')
85  ax_f.set_xlabel('frequency [THz]')
86  ax_f.set_ylabel('magnitude [arb]')
87  ax_f.set_title('DFT of tunneling current.')
88  ax_f.set_xlim([-5,100])
89
90  ax_lowf.plot(frq*1e-12,np.abs(I_f)*1e8,'b-')
91  ax_lowf.scatter(frq[lmax]*1e-12,np.abs(I_f[lmax])*1e8,marker='.',c='r')
92  ax_lowf.set_xlabel('frequency [THz]')
93  ax_lowf.set_ylabel('magnitude [arb]')
94  ax_lowf.set_title('DFT of tunneling current.')
95  ax_lowf.set_xlim([-0.1,0.1])
96
97  ax_hf.plot(frq*1e-12,np.abs(I_f)*1e8,'b-')
98  ax_hf.scatter(frq[lmax]*1e-12,np.abs(I_f[lmax])*1e8,marker='.',c='r')
99  ax_hf.set_xlabel('frequency [THz]')
100 ax_hf.set_ylabel('magnitude [arb]')
101 ax_hf.set_title('DFT of tunneling current.')
102 ax_hf.set_xlim([86.1,86.3])
103 fig_signal.tight_layout()
104
105 output = 'Signal at: '
106 for i in np.arange(int((len(lmax)/2)-0.5),len(lmax),1):
107     output = output + str(frq[lmax[i]]*1e-9) + 'GHz, '
108 output = output[:-2] + '.'
109
110 print('')
111 print(output)
112 print('')
113
114
115 '''
116 fig_d = plt.figure()
```

```
117 ax_d = fig_d.add_subplot(111)
118 ax_d.plot(frq*1e-12,np.abs(I_f)*1e8,'b-')
119 ax_d.scatter(frq[lmax]*1e-12,np.abs(I_f[lmax])*1e8,marker='x',c='red')
120 ax_d.set_title('Debugplot')
121 #ax_d.set_xlim([86.1,86.3])
122 '''
```

References

[1] T. Benschop, *Developing a high frequency current amplifier for Scanning Tunnelling Microscopy .*, Bachelor's thesis, Leiden University, 2016.

[2] S. Loth, M. Etzkorn, C. P. Lutz, D. M. Eigler, and A. J. Heinrich, *Measurement of fast electron spin relaxation times with atomic resolution.*, Science **329**, 1628 (2010).

[3] S. Baumann, W. Paul, T. Choi, C. P. Lutz, A. Ardavan, and A. J. Heinrich, *Electron paramagnetic resonance of individual atoms on a surface*, Science **350**, 417 (2015).

[4] P. Berggren and J. Fransson, *Electron Paramagnetic Resonance of Single Magnetic Moment on a Surface*, Scientific Reports **6**, 25584 (2016).

[5] W. Paul, K. Yang, S. Baumann, N. Romming, T. Choi, C. P. Lutz, and A. J. Heinrich, *Control of the millisecond spin lifetime of an electrically probed atom*, Nature Physics **13**, 403 (2017).

[6] C. F. Hirjibehedin, C.-Y. Lin, A. F. Otte, M. Ternes, C. P. Lutz, B. A. Jones, and A. J. Heinrich, *Large Magnetic Anisotropy of a Single Atomic Spin Embedded in a Surface Molecular Network*, Science **317**, 1199 (2007).

[7] Y. Manassen, R. J. Hamers, J. E. Demuth, and A. J. Castellano, *Direct Observation of the Precession of Individual Paramagnetic on Oxidized Silicon Surfaces*, Physical Review Letters **62**, 2531 (1989).

[8] U. R. Singh, R. Aluru, Y. Liu, C. Lin, and P. Wahl, *Preparation of magnetic tips for spin-polarized scanning tunneling microscopy on Fe 1 + y Te*, Physical Review B **91**, 1 (2015).

[9] F. M. Leibsle, S. S. Dhesi, S. D. Barrett, and A. W. Robinson, *STM observations of Cu(100)-c(2x2)N surfaces: evidence for attractive interactions and an incommensurate c(2 x 2) structure*, Surface Science **317**, 309 (1994).

[10] S. Loth, C. P. Lutz, and A. J. Heinrich, *Spin-polarized spin excitation spectroscopy*, New Journal of Physics **12**, 1 (2010).

[11] M. Hervé, M. Peter, and W. Wulfhekel, *High frequency transmission to a junction of a scanning tunneling microscope*, Applied Physics Letters **107**, 1 (2015).

[12] J. Bardeen, *Physical Review Letters*, Physical Review Letters **6**, 57 (1960).

[13] C. C.Gerry and P. L.Knight, *Introductory Quantum Optics*, Cambridge, 2008.

[14] J. Fransson, O. Eriksson, and A. V. Balatsky, *Theory of spin-polarized scanning tunneling microscopy applied to local spins.*, Physical Review B **81**, 1 (2010).

[15] F. Delgado, J. J. Palacios, and J. Fernandez-Rossier, *Spin-transfer torque on a single magnetic adatom*, Physical Review Letters **104**, 1 (2010).

Version of October 11, 2017– Created October 11, 2017 - 16:15